CHAPTER 4

In-Vitro bioactivity of Binuclear (II) arene complexes

The synthesized binuclear ruthenium arene complexes have been evaluated for their bio-applicability as anticancer agents, employing various assays.

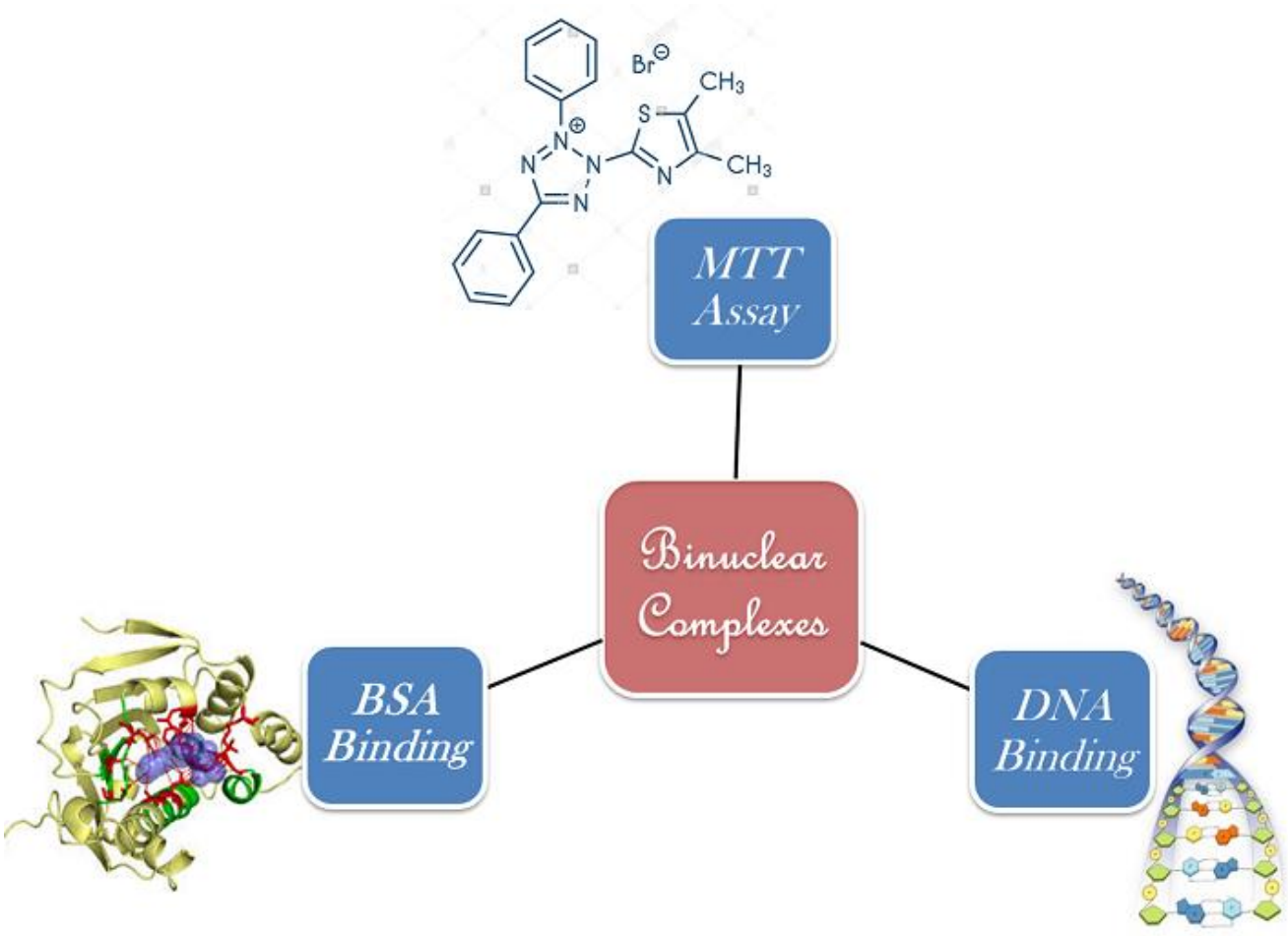

TABLE OF CONTENTS

In-Vitro assays

In-Cellulo assays

Drug Targets for Cancer Treatment:

The major steps in cell growth and division are DNA replication, transcription and protein synthesis. DNA is a major target for drug development as it is the carrier of genetic information as well as plays a major role in tumorigenesis and pathogenesis. To achieve maximum specific DNA binding affinity is always a challenge for drug development. In classical chemotherapy, anticancer agents target DNA directly according to the cisplatin paradigm, generate lesions and trigger cell death. Significant survival rate in cancer patients is observed when some of the most effective anticancer agents that target DNA are used in combination with drugs having different mechanisms of action [1]. Enzymes and proteins also contribute as major targets for anticancer drug development besides DNA and RNA, [2].

4.1 Structural diversity of metal complexes:

The transition metal complexes exhibit high degree of selectivity towards various biological targets due to their high diversity imparted by the metal ion, oxidation state, coordinated ligands, overall size and shape of the complex The structural complexity and polymorphic nature of DNA results in a number of potential intermolecular interactions, including irreversible covalent binding and non-covalent interactions such as reversible groove association or intercalation along with electrostatic interactions [2]. Metal complex-DNA interactions showcase the influence that the coordination geometry of the metal and the disposition of the ligands have on the binding activity. For example, square planar complexes permit deeper insertion of an intercalator compared to octahedral or tetrahedral geometries [3]. Various transition metal complexes can undergo vastly different binding interactions with DNA.

4.1.1 Binding of Mononuclear Metal Complexes to DNA:

4.1.1.1 Covalent bonding

Covalent binding is a common method of DNA interaction for anticancer drugs. Cisplatin and its derivatives are capable of forming various DNA adducts including the most common type, 1, 2 – intrastrand adducts in which two bonds are formed upon the same strand between consecutive base pairs.

4.1.1.2 Intercalation

The concept of intercalation was originally proposed by Lerman to explain the binding of aromatic planar molecules such as aminoacridines, exemplified by proflavine, and later phenanthridines, such as homidium bromide [4]. Intercalation involves the insertion of the planar molecule between two neighbouring base pairs of DNA stabilised by π–π stacking interactions between the base pairs and the ligand aromatic ring system which results in the lengthening, stiffening and unwinding of the DNA helix [5, 6]. Intercalation depends upon the "extent of insertion" [7-9], is reversible and stabilised by a combination of electrostatic, hydrogen bonding, entropic, van der Waals and hydrophobic interactions [10-12].

4.1.1.3 Bimodal – covalent binding and intercalation.

Many metal complexes can interact with DNA via more than one mode. Binding studies of the complex $[Pt(terpy)Cl]^+$, have revealed that this complex initially intercalates with DNA, and subsequently form covalent bonds to base pairs after the loss of the labile chloride ligand [13]. Various complexes with bimodal binding to DNA have been synthesised and some have exhibited high cytotoxicity at micromolar concentrations in the cancer cell lines [14].

4.1.2 Binding of Multinuclear complexes:

4.1.2.1 Covalent binding.

Platinum anticancer complexes consisting of two or more centres that are tethered together have attracted considerable interest as their multinuclear nature leads to the formation of a greater number of possible DNA binding adducts than cisplatin [15-17] thereby making it more difficult for cells to repair DNA damage and develop drug resistance subsequently [18,19]. Additionally, multinuclear compounds are usually charged and therefore water soluble, allowing for ease of administration, faster DNA binding and higher cellular uptake due to electrostatic attractions [15, 20, 21]. Advantage of multinuclear compounds is the variety of complexes that can be synthesised, by varying the external and tethering ligands in order to modulate the chemical properties of the complex. The external ligands influence the primary DNA binding mode, [22] while the tethering ligands influence many properties [23, 24, 25] The functional groups present and the shape of the linker can dictate the interactions between the metal complex and biomolecules [21, 26, 27] Chain length has also been found

to affect the cytotoxicity of multinuclear complexes, although trends vary depending on the rigidity of the linker [23, 28, 29].

4.1.2.2 Bimodal – covalent and groove binding.

Metal complexes with topologies that complement either the DNA major or minor groove prefer groove binding, a reversible intermolecular association [30] between the biomolecule and the complexes. These grooves are vastly different in size, shape and properties, and so association with one or the other can occur under different circumstances [31, 32]. Groove binding involves intermolecular interactions such as electrostatic and van der Waals attractions and results in relatively minor changes in the structure of the double helix [32]. Binding to the major groove of DNA is an enthalpy-driven process, while minor groove interactions are driven by entropy effects [33, 34]. Platinum complexes have been developed that bind with the grooves of DNA via non-covalent interactions before forming DNA adducts. The advantages of this bimodal interaction are an increased affinity for DNA and in some cases base sequence specificity.

4.1.2.3 Phosphate backbone association.

An intermolecular binding that may occur is association along the DNA phosphate. For example, the multinuclear complex $[\{trans\text{-}Pt(NH_3)_2(NH_2(CH_2)_6(NH_3^+))\}_2\text{-}\mu\text{-}\{trans\text{-}Pt(NH_3)_2(NH_2(CH_2)_6NH_2)_2\}]^{8+}$ (*Fig. 4.1*) [35] was reported to associate within the minor groove, and the amine protons in this complex formed hydrogen bonds with the oxygen atoms of the phosphate backbone along the DNA chain.

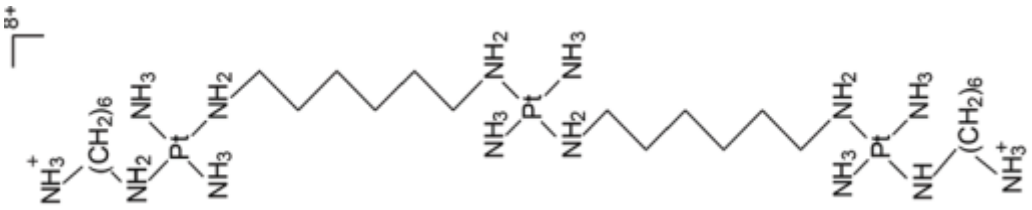

Fig. 4.1: *Structure of the multinuclear platinum (II) complex*

It has been well established in the literature that the primary cellular target for Ru (II) organometallics is DNA, which is similar to other metal-based drugs. For the family of ruthenium compounds with general formula $[Ru(\eta^6\text{-arene})(N,N')X]^+$ ($X = Cl^-$ or I^-; N, N' = ethylenediamine or N-ethylethylenediamine) DNA has been found to be the target.

Monofunctional and bifunctional adducts with DNA are formed by reaction with guanine nucleobases. The complex [Ru(biphenyl)(en)Cl]PF_6, named as RM175, binds DNA either by intercalation through the aromatic ligand or by covalent binding with the metal ion [36]. In addition to Ru(II), Ru(III) complexes with indazole moieties as ligands show interesting antitumor properties due to DNA interaction. One of the most studied Ru(III) complexes is the [Ru $(HIn)_2Cl_4$](H_2In) (HIn = indazole) (KP1019) which reacts with DNA and induces apoptosis via the intrinsic mitochondrial pathway, being accumulated mainly in cell nucleus [37]. Although the target of this compound is the same of platinum-based drugs, the induced DNA lesions are different. A variety of ruthenium complexes have been designed which interact specifically with the classical target, DNA [38, 39]. A family of ruthenium(II)-arene complexes developed by Sadler et al. [40], exhibits high in vitro and in vivo anticancer activity [41]. The direct coordinative binding of the monofunctional Ru-arene complex to N7 of G bases in DNA is complemented by intercalative binding of the biphenyl ligand and specific hydrogen bonding interactions of the ethylenediamine NH_2 groups with C_6O of guanine. These additional interactions result in unique binding modes to duplex DNA and induce different structural distortions in DNA compared to cisplatin, which may explain why these complexes are not cross-resistant with cisplatin [39]. Interestingly, this chemistry has recently been extended to include osmium (II)-arene analogues, whose hydrolytic properties can be tuned to achieve promising activity against human A549 and A2780 ovarian cancer cells [42].

Other ruthenium-based anticancer agents without arene functionality have different modes of action and specifically aim at non-classical targets such as gene products and cellular transduction pathways [43]. This shift in interest, which complements the classical approach, is one of the major trends in the field. Although much less studied than the metallodrug-DNA interactions, the interaction of metallodrugs with protein targets and the proteome deserves attention, especially since such studies will not only shed light on the mechanisms of action, but also help to identify new targets for drug therapy [38, 44].

DNA-binding studies for half-sandwich Ru(η6 -p-cymene) complexes featuring pyrazole appended ligands were investigated by electronic absorption spectroscopic titration and viscosity methods. The complexes were found to bind with CT-DNA via intrercalation with binding constant values in the order of 10^5 M^{-1}. Among the complexes, the complex with bidentate pyrazole ligand exhibited higher binding with DNA [45]. Absorption and emission

spectral studies of a series of Ru(II)-arenebipyridine and phenanthroline complexes [46] revealed that the complexes interacted with calf thymus DNA through groove binding as well as intercalative mode. Rigid dinuclear ruthenium-arene complexes showing strong DNA interactions were reported. Complexes 1-6 showed strong intercalative interaction with CT-DNA as revealed by UV-Visible spectra, fluorescence quenching experiment and CD studies [47]. The synthesis and characterization of eight ruthenium (II) complexes featuring acylthiourea ligands were reported. The complexes exhibited an intercalative mode of binding to CT-DNA, supported by circular dichroism, thiazole orange displacement and electrophoresis with pBR322 [48]. DNA binding of Ru-arene complexes of N, N′, N″-trisubstituted guanidine ligands was evaluated by UV−Visible, ethidium bromide displacement, and viscosity studies. The studies revealed that all of the complexes effectively bound with CT DNA [49].

4.1.3 Brief about the investigations in the present work:

The work presented in this chapter envisages the DNA/BSA interactions and cytotoxicity of the various binuclear Ru (II) complexes synthesised as the aim of this thesis. The synthesized ruthenium complexes have been investigated in a step-wise manner starting from the preliminary *in vitro* evaluations on interactions with the basic biomolecules like DNA and Serum albumin which were carried out outside cellular environment employing spectroscopic titration method within the cuvette. The results so obtained in these studies further prompted us to indulge in *in cellulo* studies comprising of the basic cytotoxicity evaluation on HeLa cancer cell lines and calculating corresponding IC_{50} values of complexes.

4.2 Complex-DNA interaction:

4.2.1 Interaction of Binuclear complexes with DNA:

The interactions of monometallic complexes with DNA have been investigated extensively, bimetallic complexes, wherein both metals are available for interaction with the DNA framework, have been less examined. Both bis-intercalating agents and intercalator/metal conjugates exhibit enhanced DNA binding ability in comparison to monofunctional agents. Bimetallic complexes, having both metals available for coordination to the DNA, may bind much more tightly than 2 equivalent of a corresponding monometallic complex through cooperativity from two-point binding to DNA [50].

This section describes the interaction of the synthesized bimetallic Ru (II) arene complexes with calf-thymus DNA (CT-DNA) in comparison with their ligands using absorption and fluorescence spectroscopy.

4.2.2 Materials and instrumentation:

The DNA binding studies were carried out in tris buffer (containing 15 mM tri-sodium citrate and 150 mM NaCl at pH 7.0) prepared in double distilled water. CT-DNA (calf thymus DNA) stock solution was prepared by dissolving a strand of CT-DNA in tris buffer at 4°C. The solution of CT-DNA gave a ratio of UV absorbance ~1.8 – 1.9 at 260 and 280 nm, indicating that the DNA was sufficiently free of protein [51]. The DNA concentration per nucleotide was determined by electronic absorption spectroscopy using the known molar extinction coefficient value of 6600 M^{-1} cm^{-1} at 260 nm [52]. The DNA-binding experiments were performed at 30.0°C. Stock solution of EB (ethidium bromide) was prepared in double distilled water with a concentration of 10^{-3} M. The stock solutions of all the compounds under study were prepared in DMSO with a stock concentration of 10^{-3} M. CT-DNA, Tri-sodium citrate (tris), and EB (ethidium bromide) were purchased from SRL (Sisco research laboratory, Mumbai, India.).

UV spectra were recorded on Perkin Elmer Lambda-35 dual beam UV-*Vis* spectrophotometer. Fluorescence spectra were also on JASCO FP-6300 fluorescence spectrophotometer. The data generated from the titration experiments were analyzed and plotted with the help of the software OriginPro 8.

Due to the less aqueous solubility of the metal complexes, DNA/BSA binding and cytotoxicity studies were carried out using stock solutions of the complexes prepared in DMSO. The solutions were then diluted with tris buffer so that the test solutions contained no more than 1% DMSO. To check the stability of the complexes in DMSO, UV-Visible spectra of the complexes **C1–C8** were recorded at room temperature in the range 200–500 nm at time intervals up to 48 h. No changes in the UV-Vis spectra were observed, implying that the complexes are stable in DMSO solution.

4.2.3 Experimental:

If a compound is suspected of targeting cellular DNA, a battery of simple *in vitro* experiments can be performed to readily determine whether the compound physically

interacts with DNA. Together, these assays are powerful tools to determine the mechanism of previously discovered molecules, and will be crucial to the discovery of the next generation of DNA-binding anticancer drugs. Two such techniques: (i) UV-Vis absorption studies and (ii) Competitive binding studies with EB using fluorescence spectroscopy; have been exploited the most for studying DNA binding with synthesized molecules. These are spectroscopy based titration methods.

4.2.3.1 UV absorption studies:

Absorption spectroscopy has been used to detect the interactions between the biological macromolecule DNA and compounds under study. The binding efficiency of a metal complex to DNA can be effectively investigated employing electronic spectroscopy since the observed changes in the spectra may give evidence of the existing interaction mode [53]. Any interaction between the compounds and DNA is expected to perturb the ligand or metal centred transitions of the compounds. Binding with DNA via non-intercalative binding modes, such as electrostatic forces, van der Waals interactions, dative bonds, hydrogen bonds and hydrophobic interactions generally results in increase in absorption intensity (hyperchromism) upon increasing the concentration of CT-DNA. DNA possesses several hydrogen bonding sites which are accessible both in minor and major grooves, it is likely that the amine or hydroxyl groups of the test compounds form hydrogen bonds with N-3 of adenine or O-2 of thymine in the DNA, which may contribute to the hyperchormism observed in the absorption spectra. The hyperchromic effect may also be due to the electrostatic interaction between positively charged compound and the negatively charged phosphate backbone at the periphery of the double helix CT-DNA [54]. If the binding mode is intercalation, the π^* orbital of the intercalated ligand can couple with the π orbital of the DNA base pairs, thus, decreasing the $\pi \rightarrow \pi^*$ transition energy and resulting in the bathochromism. On the other hand, the coupling π orbital is partially filled by electrons, thus, decreasing the transition probabilities and concomitantly resulting in hypochromism. It is a general observation that the binding of an intercalative molecule to DNA is accompanied by hypochromism and significant redshift (bathochromism) in the absorption spectra due to strong stacking interaction between the aromatic chromophore of the ligand and DNA base pairs with the extent of hypochromism and red-shift commonly consistent with the strength of intercalative interaction [55, 56].

To evaluate the interaction of the complexes with calf thymus DNA, the absorption spectral experiments were conducted in Tris-HCl/NaCl buffer (5 mM Tris-HCl, 5 mM NaCl) having pH 7.2 and using stock solution of the complexes (1 mM) in DMSO at an ambient temperature. Absorption studies were carried out by keeping fixed concentrations of complexes and varying the concentration of CT-DNA. Solutions of the 20 μL complexes were taken from the stock solution prepared as mention above and further it were diluted with 980 μL tris buffer to obtain the desired concentration. The overall volume of the cuvette was kept 1000 μM. While measuring the absorption of the complexes, equal increments of CT-DNA solution were added to both the sample cell and to the reference cell in order to eliminate the absorbance of CT-DNA itself. The binding constant (K_b) of the complexes to DNA were calculated using the McGhee-von Hippel (MvH) method [57].

$$\mathbf{[DNA] / (\varepsilon_A-\varepsilon_f) = [DNA]/(\varepsilon_b-\varepsilon_f)+1/K_b(\varepsilon_b-\varepsilon_f)} \qquad \mathbf{(4.1)}$$

Where [DNA] is the concentration of DNA in base pairs, $\varepsilon_A = A_{obsd}/$ [compound], ε_f is the extinction coefficient for the unbound compound and ε_b is the extinction coefficient for the compound in the fully bound form. $\boldsymbol{K_b}$ (binding constant) is given by the ratio of slope to the *y* intercept in plots $[DNA]/(\varepsilon_A-\varepsilon_f)$ *versus* [DNA] according to equation **(4.1)**. The UV absorption spectra of representative ligands and complexes have been shown in Fig. 4.1 & 4.2.

The standard Gibb's free energy for DNA binding was calculated from the relation (**4.2**) [58]

.

$$\mathbf{\Delta G^{\circ}_b = -RT \ln K_b} \qquad \mathbf{(4.2)}$$

Where ΔG° Standard change in Gibb's free energy, R is universal gas constant (8.314 JK^{-1} mol^{-1}), T is temperature in Kelvin, ln K is natural log of K while K is equilibrium constant.

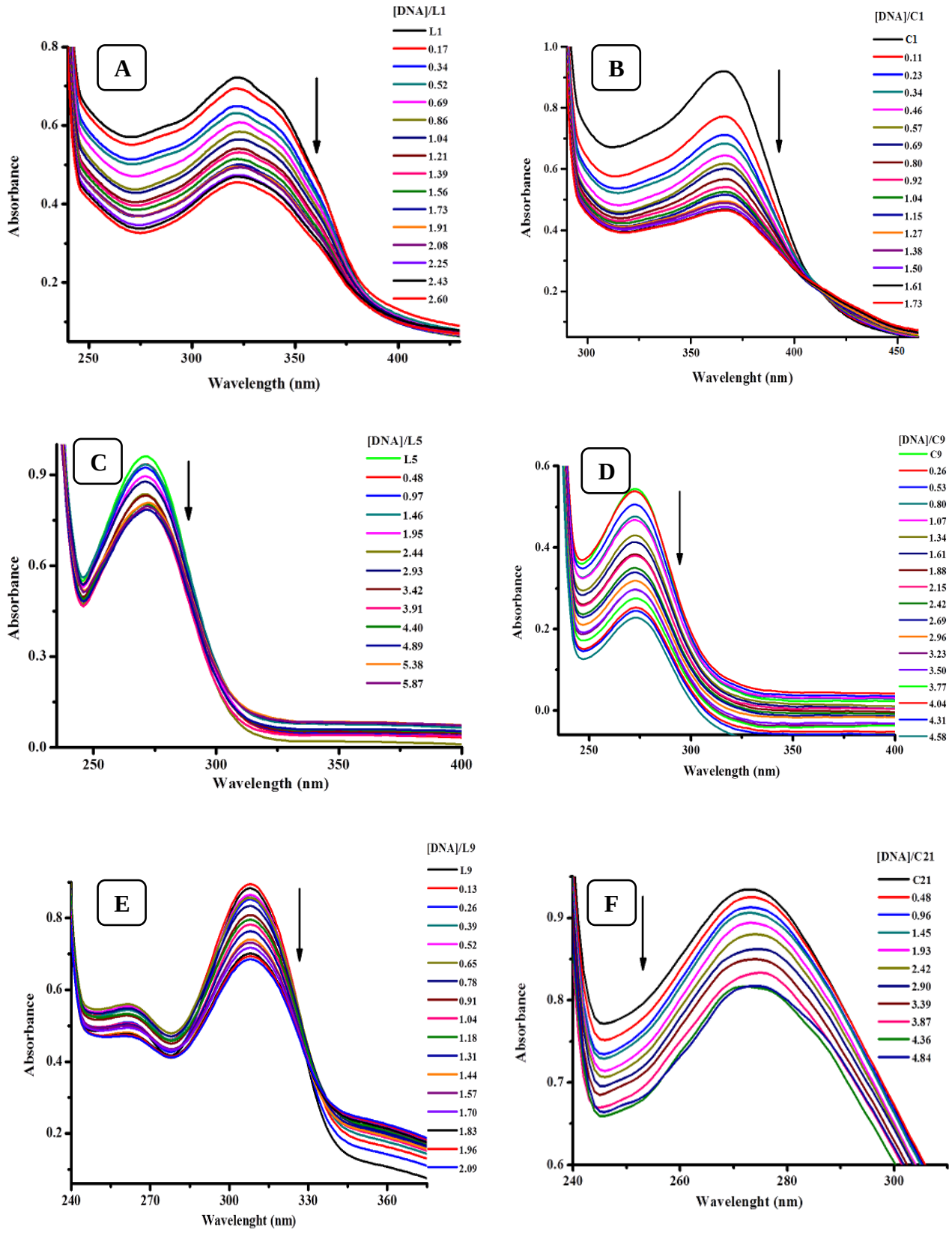

Fig. 4.2: *UV absorption spectra of representative ligands and complexes (A)* ***L1*** *(B)* ***C1*** *(C)* ***L5*** *(D)* ***C9*** *(E)* ***L9*** *and (F)* ***C21*** *at increasing concentrations of CT-DNA, the arrow shows decrease in intensity upon increasing concentration of the DNA*

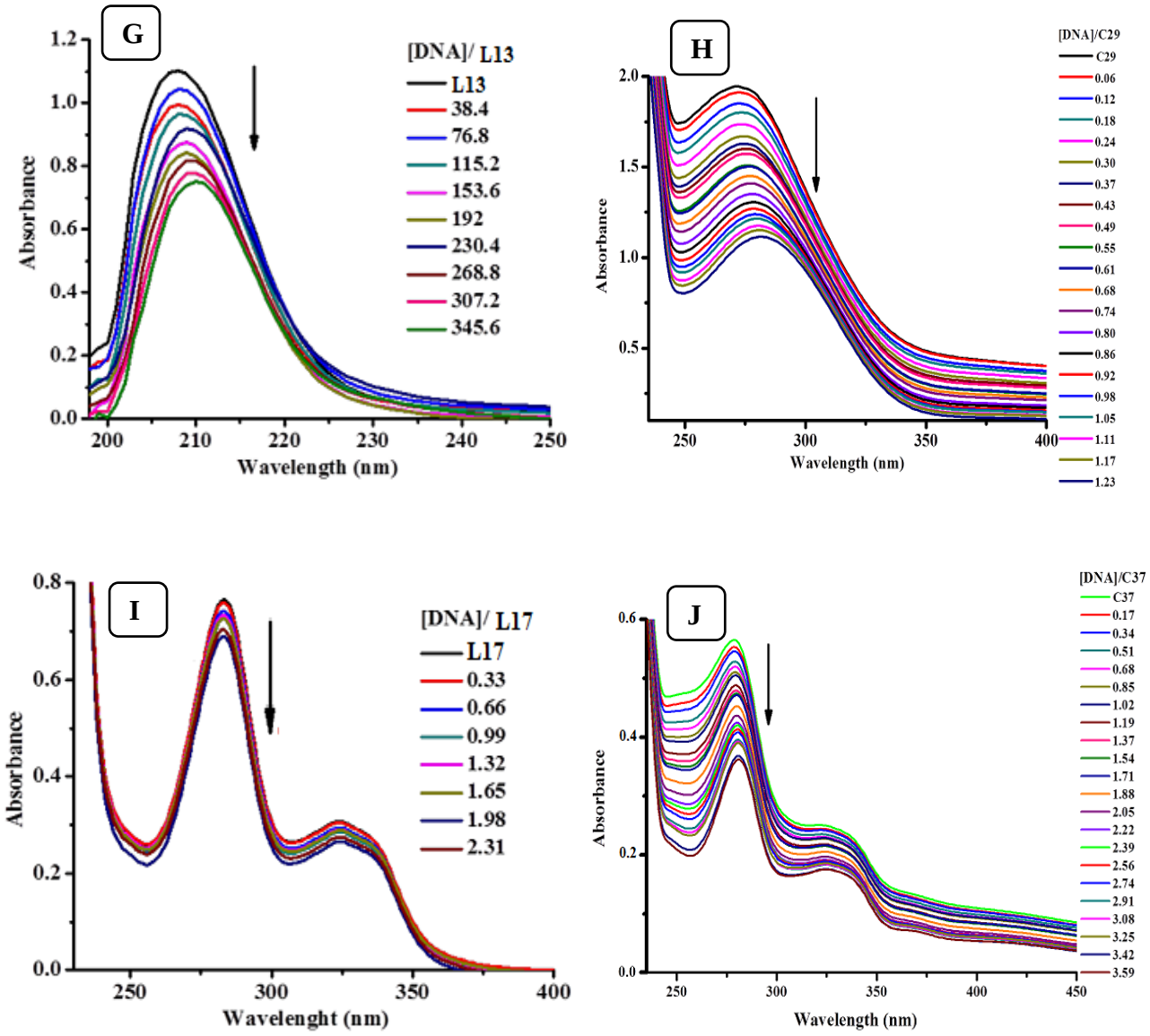

Fig. 4.3: (Cont...): *UV absorption spectra of representative ligands and complexes (G)* ***L13*** *(H)* ***C29*** *(I)* ***L17*** and *(J)* ***C37*** *at increasing concentrations of CT-DNA, the arrow shows decrease in intensity upon increasing concentration of the DNA*

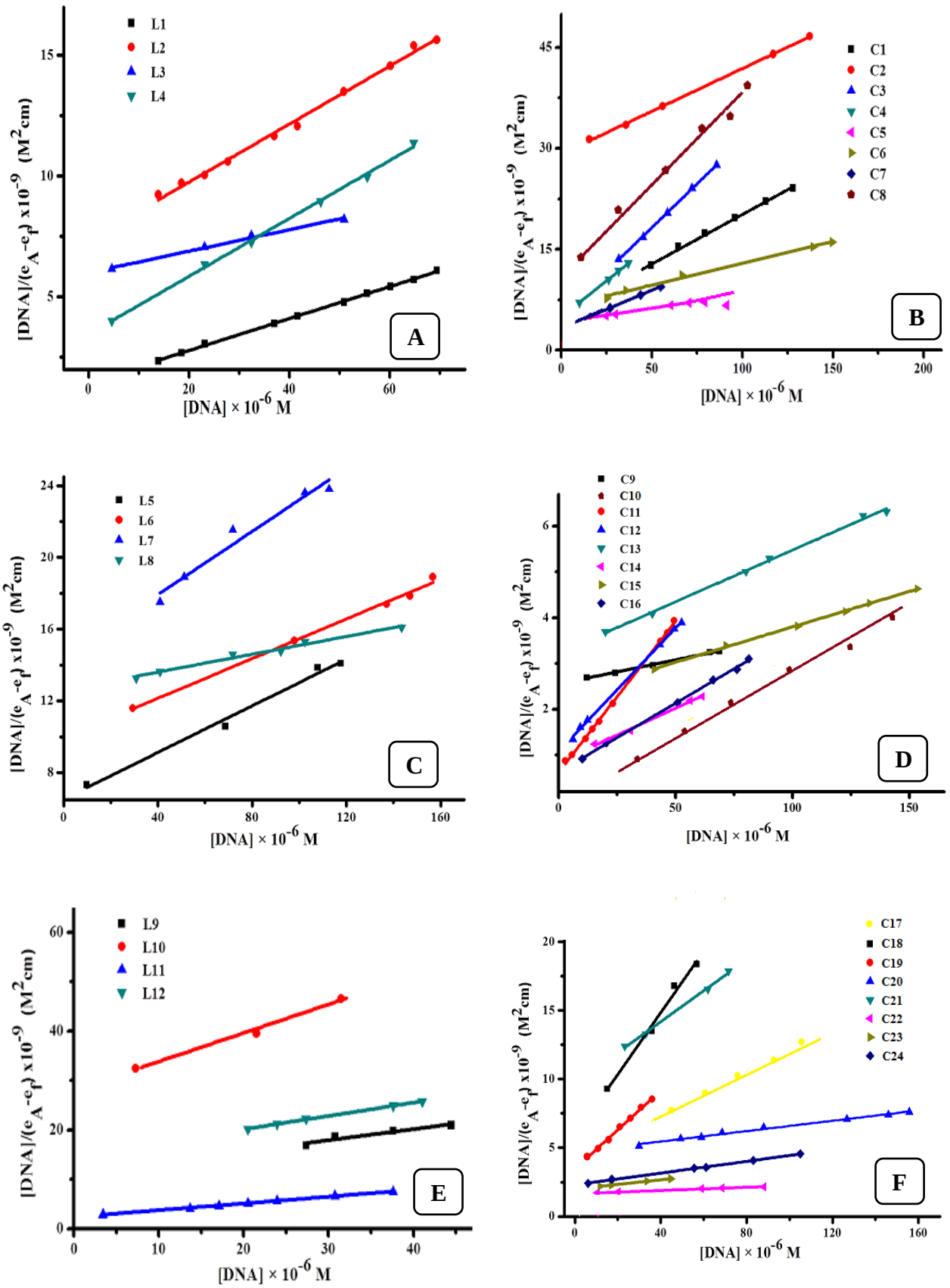

Fig. 4.4: *Plot of [DNA]/(ε_A -ε_f) versus [DNA] for (A)* ***L1-4*** *(B)* ***C1-C8*** *(C)* ***L5-8*** *(D)* ***C9-16*** *(E)* ***L9-12*** *and (F)* ***C17-24***

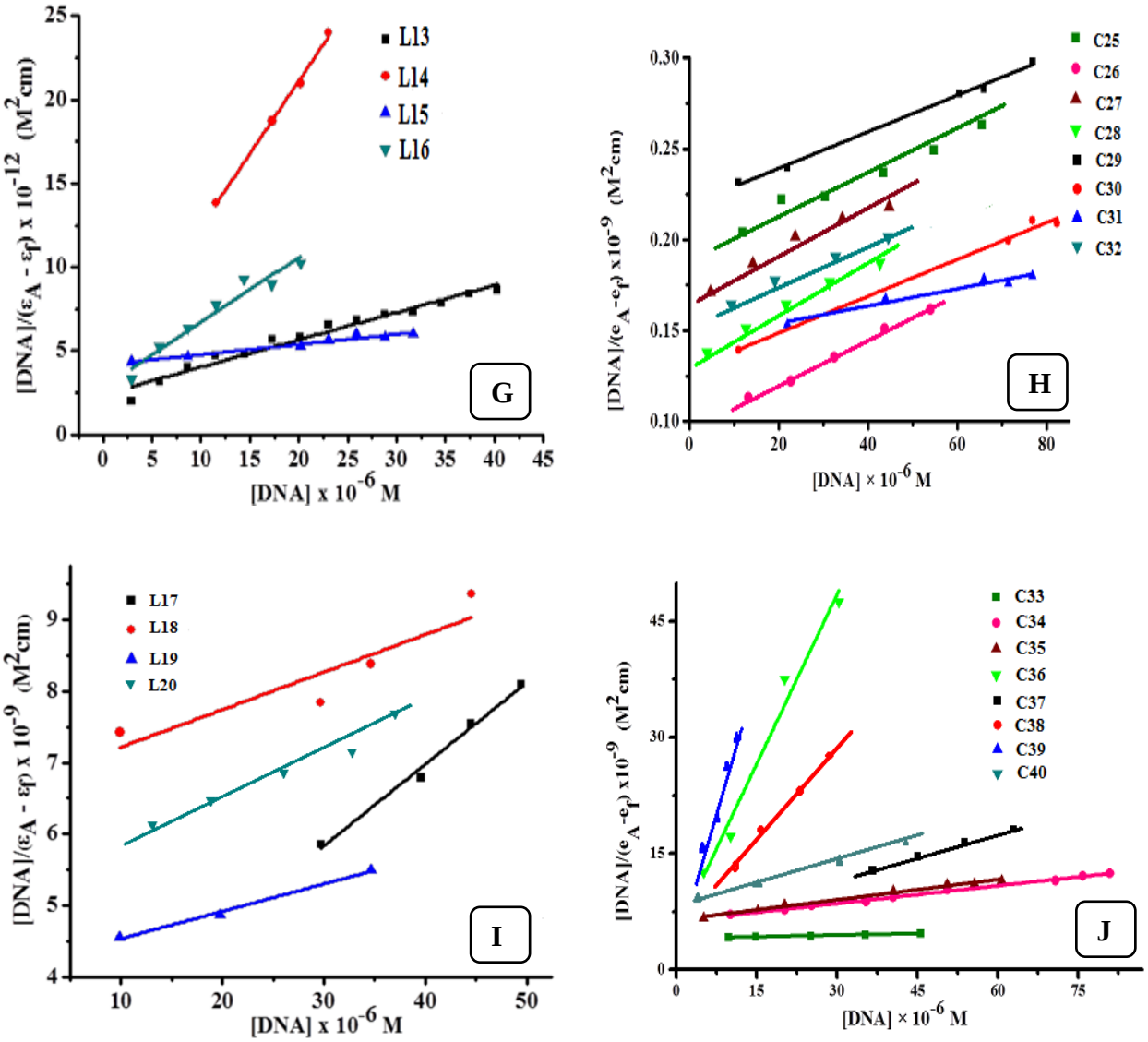

Fig. 4.5: (Cont...): *Plot of [DNA]/(ε_A -ε_f) versus [DNA] for (G)* ***L13-16*** *(H)* ***C25-32*** *(I)* ***L17-20*** and *(J)* ***C33-40***

The [DNA]/(ε_A -ε_f) versus [DNA] plots for all the synthesized binuclear Ru(II) complexes have been shown in *Fig. 4.4* and *4.5* $\boldsymbol{K_b}$ values obtained from these plots have been tabulated and discussed with significance to their structures in section 4.2.4.

4.2.3.2. Competitive binding studies with EB using fluorescence spectroscopy:

In order to examine the ability of the compounds to displace EB from its DNA-EB complex, a competitive EB binding study has been undertaken employing fluorescence experiments [59]. Ethidium Bromide (EB = 3,8-diamino-5-ethyl-6-phenyl-phenanthridinium bromide) a

phenanthridine fluorescent dye is a typical indicator of intercalation, forming soluble complexes with nucleic acids and emitting intense fluorescence in the presence of DNA due to the intercalation of the planar phenanthridinium ring between adjacent base pairs on the double helix [60, 61]. The displacement of EB (quantified by fluorescence) by the addition of a compound is suggestive of an intercalative binding [62, 63]. Addition of a second molecule (compound under study), which may replace EB from the DNA-EB complex results in a decrease of the DNA-induced EB emission due to displacement of EB from the intercalation sites of DNA [64].

Fluorescence spectroscopy was employed to examine whether the complexes have the ability to displace EB from DNA–EB complex and to confirm the intercalative mode of binding of the complexes. The titration experiment was carried out by keeping the DNA-EB complex concentration constant and varying the complex concentration. The DNA–EB complex was prepared by adding EB (33.3 µM) and CT-DNA (20 µM) in tris buffer in the cuvette. The variation in the fluorescence emission spectrum of the DNA–EB complex was recorded by addition of aliquot of the complexes. The fluorescence emission (λ_{ex} = 520 nm) was measured from 530 nm to 700 nm using 5 nm slits. The titration curves so generated have been representatively shown for each series in *Figs. 4.6* and *4.7*.

The relative binding of complexes to CT-DNA was determined by calculating the quenching constant ($\boldsymbol{K_{SV}}$) from the slopes of straight lines obtained from the Stern-Volmer equation **(4.3)** [65].

$$\mathbf{Io/I = 1 + K_{SV}\,[Q]} \qquad \mathbf{(4.3)}$$

where Io and I are the emission intensities in the absence and the presence of the quencher (Q = compound) respectively, [Q] is the concentration of the quencher and $\boldsymbol{K_{SV}}$ is the Stern Volmer constant which can be obtained from the slope of the plot of Io/I *versus* [Q] and is often used to evaluate the quenching efficiency of each compound. The $\boldsymbol{K_{SV}}$ plots for the representative ligands and their corresponding Ru (II) complexes have been shown in *Figs. 4.8 and 4.9.* The $\boldsymbol{K_{SV}}$ values obtained from these plots have been tabulated and discussed in section 4.2.4. The standard deviation (SD) for $\boldsymbol{K_b}$ and $\boldsymbol{K_{SV}}$ are calculated and tabulated in their respective tables given below.

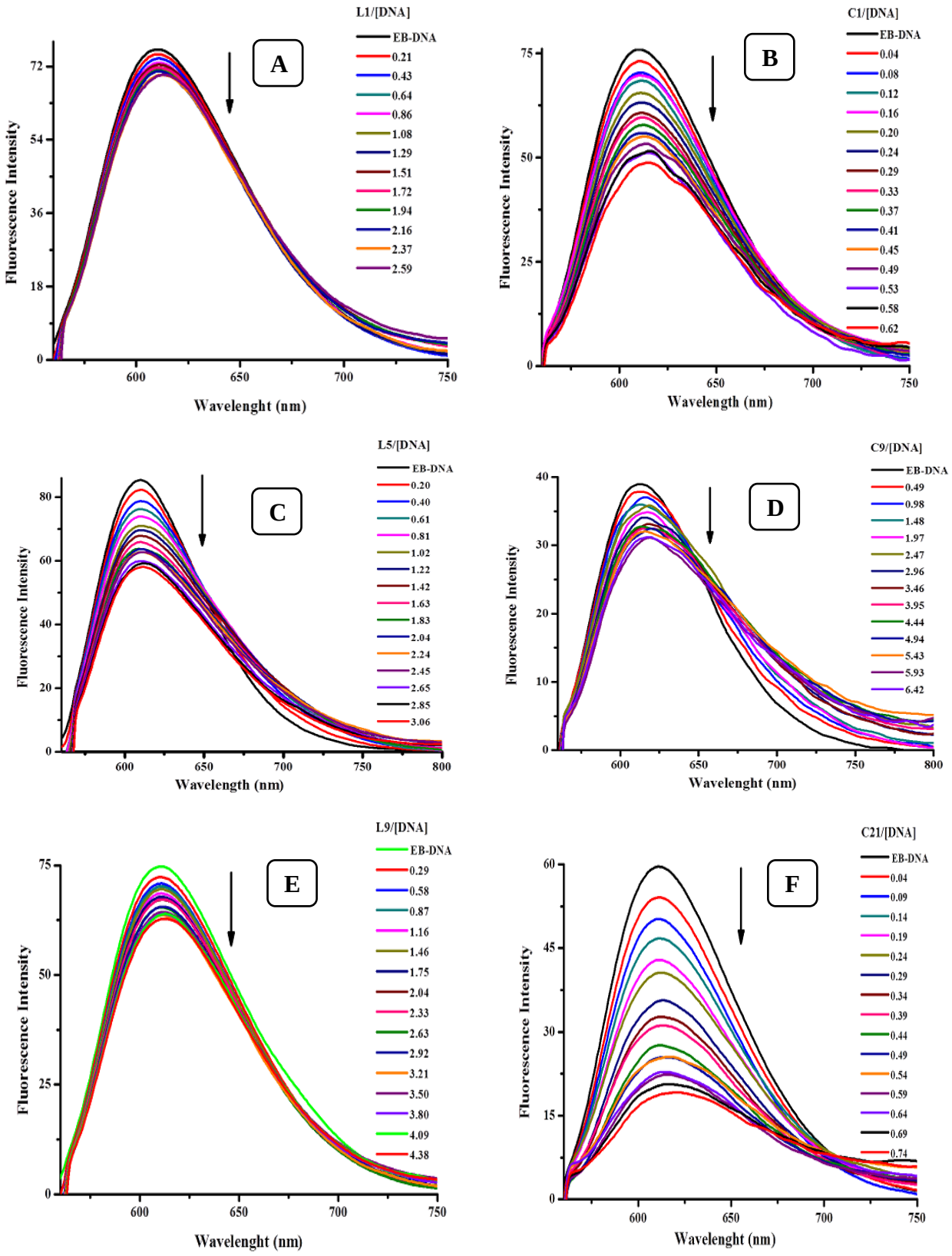

Fig. 4.6: *Fluorescence emission spectra of EB-DNA complex at increasing concentrations of representative ligands and complexes (A)* ***L1*** *(B)* ***C1*** *(C)* ***L5*** *(D)* ***C9*** *(E)* ***L9*** and *(F)* ***C21;*** *arrow shows decrease in intensity (quenching of DNA-EB fluorescence) upon increasing the concentration of the compounds*

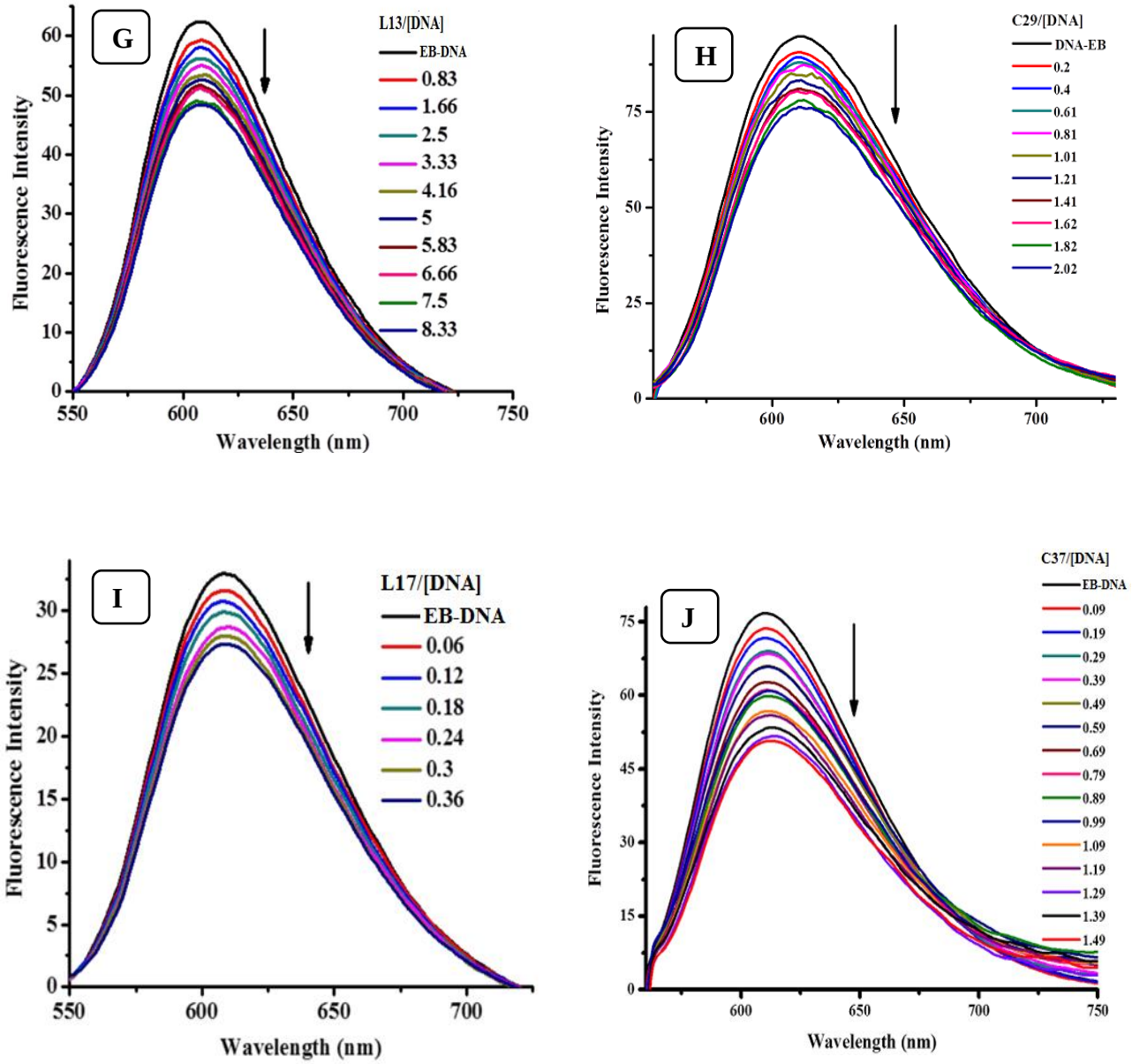

Fig. 4.7: (Cont...): *Fluorescence emission spectra complex at increasing concentrations of (G)* ***L13*** *(H)* ***C29*** *(I)* ***L17*** and *(J)* ***C37*** *the arrow shows decrease in intensity (quenching of DNA-EB fluorescence) upon increasing concentration of the compounds*

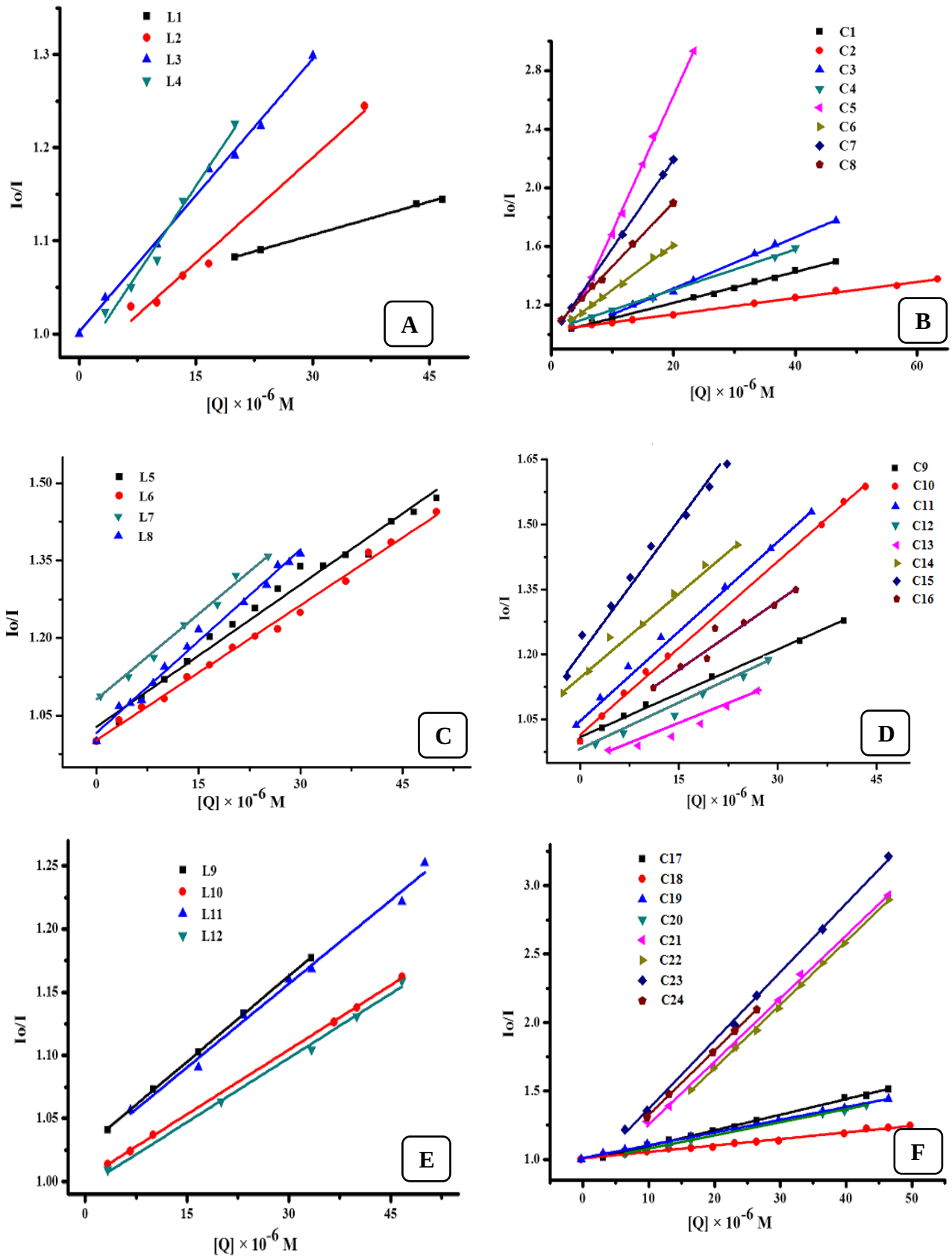

Fig. 4.8: *Stern-Volmer quenching plot Io/I versus [Q] of EB-DNA for (A)* ***L1-4*** *(B)* ***C1-8*** *(C)* ***L5-8*** *(D)* ***C9-16*** *(E)* ***L9-12*** *and (F)* ***C17-24***

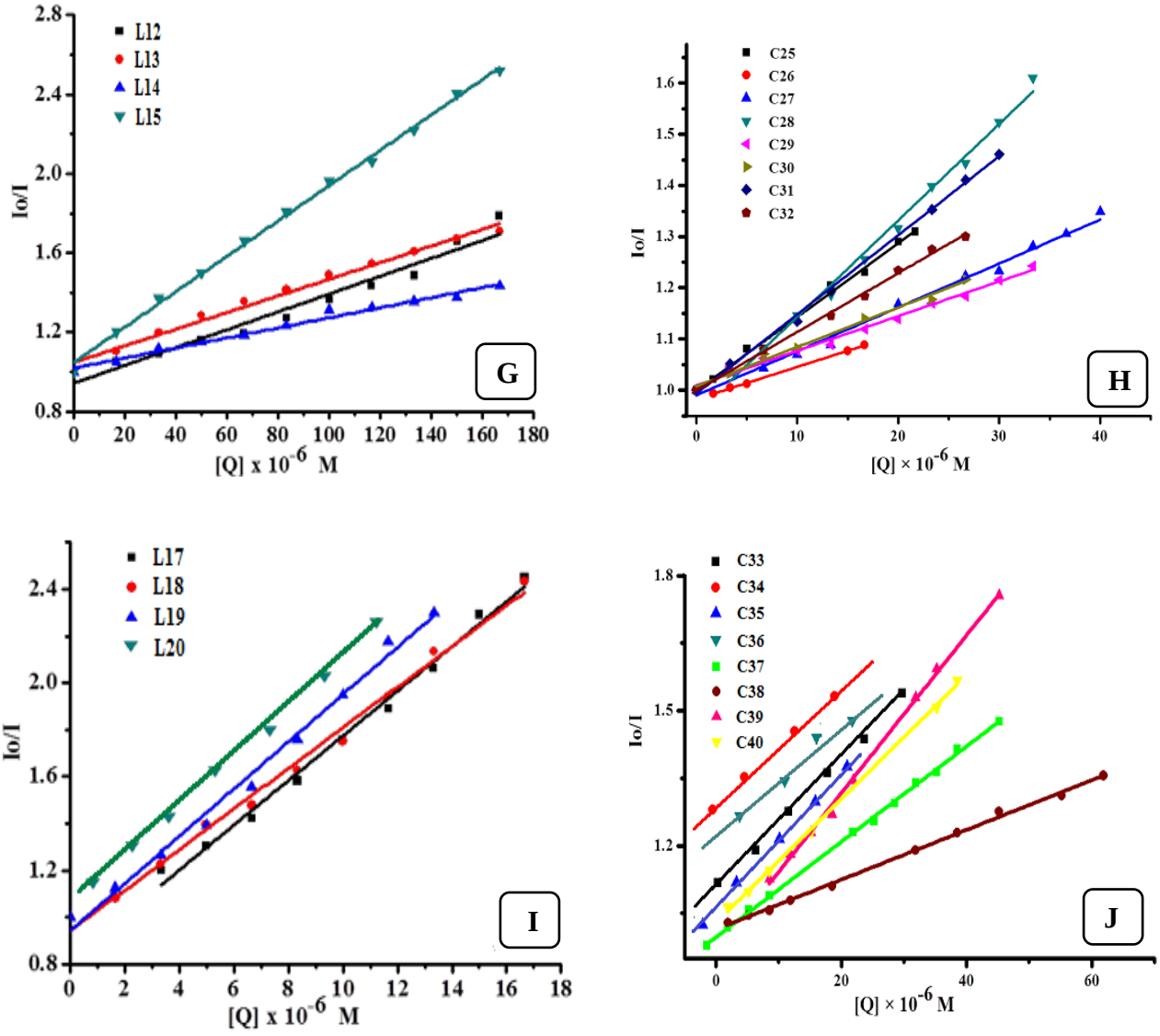

Fig. 4.9: (Cont...): *Stern-Volmer quenching plot Io/I versus [Q] of EB-DNA for (G)* ***L12-15*** *(H)* ***C25-32*** *(I)* ***L17-20*** and *(J)* ***C33-40***

4.2.3.3. Viscosity measurement:

The viscosity of DNA is sensitive to length changes and is regarded as the least ambiguous and the most critical clue of a DNA binding mode in solution [66]. In general; intercalating agents are expected to elongate the double helix to accommodate the ligands in between the base pairs, leading to an increase in the viscosity of DNA. In contrast, a complex that binds exclusively in the DNA grooves typically causes less pronounced (positive or negative) or no changes in DNA solution viscosity [67, 68].

Cannon–Ubbelohde viscometer was used to measure the relative viscosity of DNA. The viscosity measurements of DNA (200 μM) solutions were carried out at a constant temperature of 32.0 ± 0.1 ºC in the presence of complexes at [complex]/[DNA] ratio of 0, 0.04, 0.08, 0.12, 0.16 and 0.20 in Tris–HCl buffer (pH 7.2). Digital stopwatch with least count of 0.01 s. was used for flow time measurement with accuracy of ±0.1 s. The flow time of each sample was measured three times and an average flow time was calculated. Data are presented as $(\eta/\eta_0)^{1/3}$ *versus* [complex] / [DNA], where η is the viscosity of DNA in the presence of complex and η_0 is the viscosity of DNA alone. Viscosity values were calculated from the observed flow time of DNA-containing solutions (t) corrected for that of the buffer alone (t_0), $\eta = (t-t_0)/t_0$ [69].

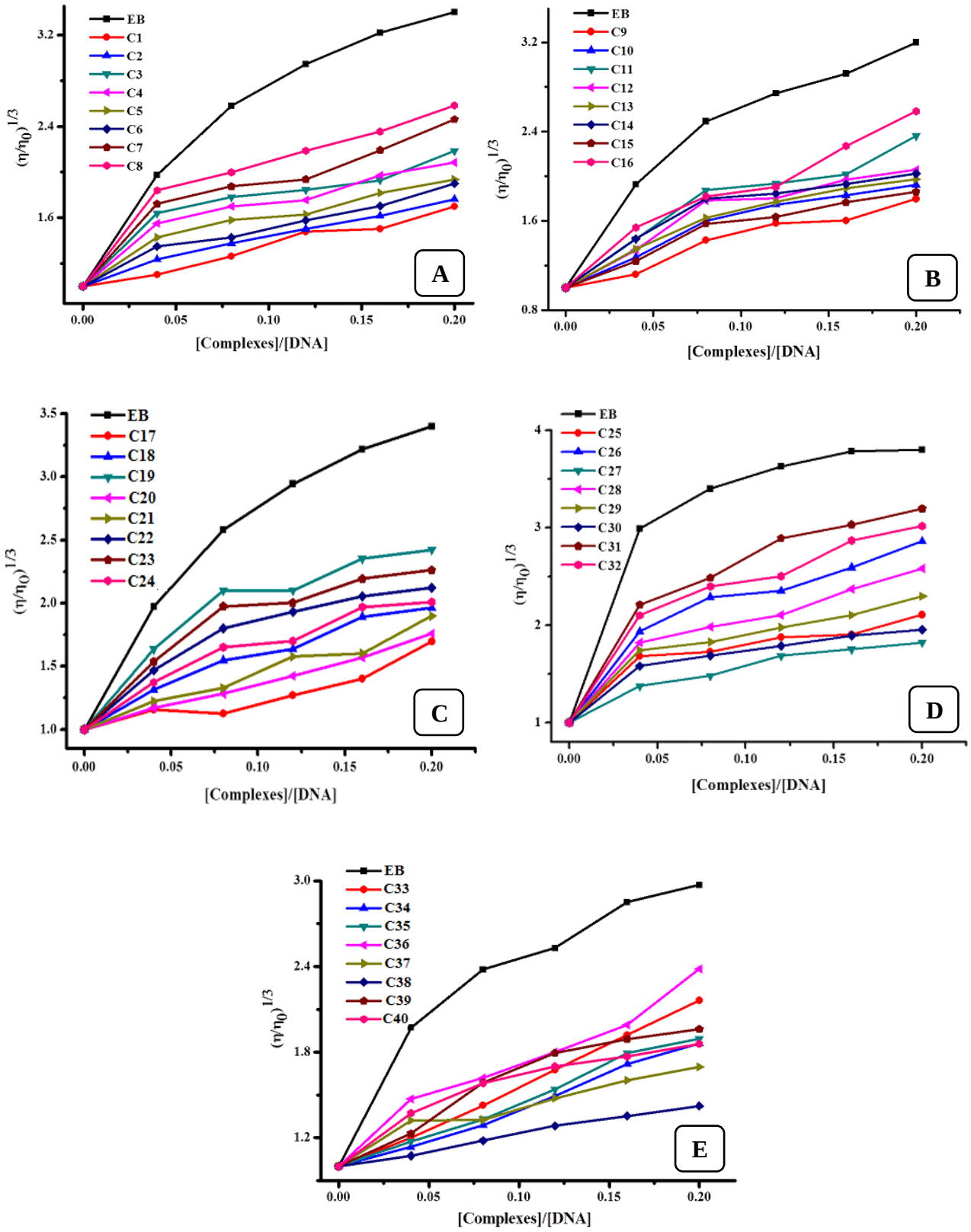

Fig. 4.10: *Effect of increasing amounts of the complexes (A)* ***C1-8*** *(B)* ***C9-16*** *(C)* ***C17-24*** *(D)* ***C25-32*** and *(E)* ***C33-40*** *and Ethidium Bromide (****EB****) on the relative viscosity of CT-DNA (200µM) in Tris-HCl buffer at 32 (± 0.1) °C. [Complex]/[DNA] = 0, 0.04, 0.08, 0.12, 0.16 and 0.2*

4.2.4 Results and discussion:

4.2.4.1 *Diphenyl pyrazol thiosemicarbazones Series:*

The K_b (intrinsic binding constant) values (Table 4.1) obtained from the plot of [DNA]/(ε_A-ε_f) *versus* [DNA] (*Fig. 4.4* A, B) using equation **(4.1)** are in the order of 10^3 M^{-1} for the thiosemicarbazones **L1-4,** 10^4 M^{-1} for the imidazole bridged complexes **C1-4** and 10^4-10^5 M^{-1} for the azopyridine bridged complexes **C5-8**, suggesting moderate binding of the ligands and strong binding of their complexes to CT-DNA. An observed hypochromism along with a bathochromic shift is indicative of intercalative mode of binding to the DNA. The ruthenium complexes **C7** and **C8** with 4, 4'- azopyridine as a bridging ligand shows the highest K_b values of 1.1 x 10^5 M^{-1} and 1.2 x 10^5 M^{-1} respectively; among the complexes with imidazole as a bridging ligand **C3** shows the highest K_b value (7.2 x 10^4 M^{-1}). The binding constants are in the order of **C8>C7>C3>C4 >C2>C1>C5>C6.** An overall comparison of the K_b values show that the complexes with additional hydrophobic arene moieties in the pyrazole derivatives are relatively better DNA binders due to stronger interactions. Competitive EB binding studies show quenching of EB–DNA fluorescence on titration with the ligands and complexes suggesting that the compounds displace EB from the EB–DNA complex and interact with DNA via intercalative mode. The Stern–Volmer quenching plots of EB–DNA (*Fig. 4.8* A, B) illustrate that the quenching of EB bound to DNA by the compounds is in good agreement (R = 0.97 – 0.98) with the linear Stern–Volmer equation **(4.2)**. The K_{SV} values of the compounds given in Table 4.1 show that they have good affinity for DNA with values in the range of 1.2 – 9.8 x 10^3 M^{-1} for **L1-4** and 1.3 – 9.2 x 10^4 M^{-1} for **C1-8**. It can be well noted that the complexes show 10 fold better displacement efficacies of EB from EB-DNA complex than the diphenyl pyrazol thiosemicarbazones ligands. This observation is in line with the K_b values obtained from UV absorption studies. The K_{SV} values show that **C5** and **C7** with azopyridine bridge have the maximum quenching efficiency among all the complexes in this series. The free energy change ΔG° values for the binding interactions calculated from equation **4.2** are included in Table 4.1.

In order to further confirm the mode of binding of the complexes **C1-8** to CT-DNA**,** viscosity measurements of DNA solutions were carried out in presence and absence of the complexes. In general, intercalating agents are expected to elongate the double helix to accommodate the complexes in between the base pairs, leading to an increase in the viscosity of DNA. In contrast, a complex that binds exclusively in the DNA grooves typically causes less

pronounced (positive or negative) or no changes in DNA solution viscosity. The effects of the complexes and classical intercalator EB on the viscosities of CT-DNA solution are shown in *Fig. 4.10* (A). With increasing [complex]/ [DNA] concentration ratios, (*[Complex]/ [DNA] = 0, 0.04, 0.08, 0.12, 0.16 and 0.20)*, the relative viscosities of CT-DNA increased gradually indicative of characteristic intercalative mode of binding which is in accordance with previous findings.

Table 4.1 : *DNA binding constants of* ***L1-4***, ***C1-4*** *and* ***C5-8***

Code	***DNA binding constant***			
	$K_b\ M^{-1}$	$K_{SV}\ M^{-1}$	***λ shift***	**ΔG° kJmol^{-1}**
L1	$4.5 \times 10^3 \pm 0.021$	$2.3 \times 10^3 \pm 0.0283$	-	−20.84
L2	$1.1 \times 10^3 \pm 0.023$	$7.5 \times 10^3 \pm 0.0507$	1 nm	−17.35
L3	$7.4 \times 10^3 \pm 0.031$	$9.8 \times 10^3 \pm 0.056$	-	−22.07
L4	$2.3 \times 10^3 \pm 0.023$	$1.2 \times 10^3 \pm 0.082$	1 nm	−19.18
C1	$2.8 \times 10^4 \pm 0.007$	$1.1 \times 10^4 \pm 0.035$	2 nm	−25.37
C2	$4.6 \times 10^4 \pm 0.009$	$5.5 \times 10^4 \pm 0.027$	1nm	−26.60
C3	$7.2 \times 10^4 \pm 0.017$	$1.7 \times 10^4 \pm 0.036$	1 nm	−27.71
C4	$6.8 \times 10^4 \pm 0.041$	$1.3 \times 10^4 \pm 0.042$	1 nm	−27.57
C5	$2.6 \times 10^4 \pm 0.026$	$9.2 \times 10^4 \pm 0.036$	2 nm	−25.19
C6	$1.6 \times 10^4 \pm 0.012$	$3.1 \times 10^4 \pm 0.028$	3nm	−23.98
C7	$1.1 \times 10^5 \pm 0.032$	$6.0 \times 10^4 \pm 0.036$	2nm	−28.76
C8	$1.2 \times 10^5 \pm 0.12$	$4.3 \times 10^4 \pm 0.042$	1nm	−28.98

4.2.4.2 *Diphenylpyrazol α-amino acid derivatives:*

DNA binding constant K_b for diphenylpyrazole α-amino acid derivatives **L5-8** and their complexes **C9-16** were obtained in the range of 2.4 – 8.8 x 10^4 M^{-1} and 1.0 – 6.6 x 10^4 M^{-1} respectively from the decay of absorbance (Table 4.2). The absorption bands (*Fig. 4.2* C, D) of the ligands **L5-8** and the complexes **C9-16** showed hypochormism as well as bathochromism. It can be seen that **L7** and **C11** show slightly higher binding values among the ligands and the complexes respectively. The observed enhanced binding of these compounds may be attributed to the presence of electron releasing methyl group in the

Table 4.2 : *DNA binding constants of* ***L5-8***, ***C9-12*** *and* ***C13-16***

Code	***DNA binding constant***			
	$K_b\ M^{-1}$	$K_{SV}\ M^{-1}$	***λ shift***	**ΔG° kJmol^{-1}**
L5	6.5 x 10^4 ± 0.011	9.2 x 10^3 ± 0.034	-	−27.46
L6	5.5 x 10^4 ± 0.008	8.7 x 10^3 ± 0.036	-	−27.04
L7	8.8 x 10^4 ± 0.012	9.8 x 10^4 ± 0.048	1 nm	−28.21
L8	2.4 x 10^4 ± 0.011	1.1 x 10^4 ± 0.056	2 nm	−25.18
C9	1.0 x 10^4 ± 0.021	6.8 x 10^4 ± 0.046	2 nm	−22.82
C10	4.3 x 10^4 ± 0.045	1.3 x 10^4 ± 0.039	2 nm	−26.43
C11	6.6 x 10^4 ± 0.034	9.7 x 10^4 ± 0.047	1 nm	−27.49
C12	5.4 x 10^4 ± 0.028	2.3 x 10^4 ± 0.022	2 nm	−27.00
C13	2.1 x 10^4 ± 0.012	8.2 x 10^4 ± 0.032	2 nm	−24.66
C14	2.3 x 10^4 ± 0.024	5.1 x 10^4 ± 0.018	-	−24.88
C15	1.6 x 10^4 ± 0.090	9.0 x 10^4 ± 0.037	-	−23.98
C16	3.0 x 10^4 ± 0.017	7.2 x 10^4 ± 0.084	1nm	−25.54

leucine derivative, making the interactions more facile [70] Moreover the K_{SV} values also point towards the same conclusion as discussed above. Overall both the diphenylpyrazol α-amino acid derivatives and their binuclear ruthenium (II) complexes show moderate binding towards DNA probably through intercalation. The magnitude of binding strength to CT-DNA determined through the calculation of binding constants K_b (obtained from plots in (*Fig. 4.4* C, D) have been tabulated in Table 4.2. The Stern—Volmer quenching plots illustrate that quenching of fluorescence of the EB —DNA complex is in good agreement (R=0.94–0.98) with the linear Stern–Volmer equation. If the binding mode of the ligands/complexes with DNA is intercalation, the compounds will remove EB from the binding sites of DNA which should decrease the fluorescence of the EB-DNA complex as observed (*Fig. 4.6* C, D) [71]. The K_{sv} values are in the range of 2.4 – 8.8 x 10^4 for the ligands and 1.3 – 9.7 x 10^4 for the complexes. The complexes are slightly better quenchers from their ligand counterparts in some cases but not all. The ΔG values for the binding interactions are given in Table 4.2. The effect of the complexes on the viscosities of CT-DNA solution are shown in *Fig. 4.10* (B) Increasing [complex]/[DNA] concentration ratios gradually increased the relative viscosity of CT-DNA solution which is the characteristic of intercalative mode of binding in accordance with literature studies [67, 68].

4.2.4.3 *Ferrocenyl thiosemicarbazone series:*

The *n*→π* bands of ligands **L9-12** and their complexes **C17-24** showed hypochormism with a slight red shift on the addition of increasing amounts of DNA solution. The binding constants K_b (obtained from plots in *Fig. 4.2 E, F*) and the ΔG values have been tabulated in Table 4.3. K_b values for the ligands **L9-12** are in the range of 1.5 x 10^3– 2.0 x 10^4 M^{-1} indicative of moderate binding of the ligands with CT- DNA. The complexes **C17, C18** and **C19** ($\mathbf{K_b}$ = 3.1 x 10^4, 6.7 x 10^4 and 1.8 x 10^4 M^{-1} respectively) showed 10 fold better DNA binding than their corresponding ligands while **C20** exhibited low binding efficacy because of the presence of bulky naphthyl group which may hinder intercalation partially**. C21–24** showed good binding to DNA with binding values in the range of 9.6 x 10^3 – 2.8 x 10^4 M^{-1}. It is observed that the complexes **C19** and **C23** with 4-phenyl substituted thiosemicarbazone ligand show the highest binding affinity due to the presence of additional hydrophobic group which facilitates interaction with DNA. In contrast **C20** with 4-napthyl substitution shows lowest K_b value due to bulky napthyl group which may cause steric hindrance to intercalation. **C18** and **C22** display good binding affinities due to electron releasing 4-methyl

substitution which facilitates binding. A fluorescent EB displacement assay was performed in order to further confirm intercalative binding between the complexes and DNA. The Stern–Volmer quenching plots (*Fig. 4.8* E, F) illustrate that the quenching of EB bound to DNA by ferrocenyl thiosemicarbazones and their ruthenium complexes are in good agreement (R = 0.97 – 0.98) with the linear Stern–Volmer equation. The Stern-Volmer quenching constant K_{SV} values have been tabulated in Table 4.3.

Table 4.3 : *DNA binding constants of* ***L9-12***, ***C17-20*** *and* ***C21-24***

Code	***DNA binding constant***			
	$K_b\ M^{-1}$	$K_{SV}\ M^{-1}$	***λ shift***	**ΔG° kJmol^{-1}**
L9	2.0 x 10^4 ± 0.028	4.5 x 10^3 ± 0.049	1 nm	–24.54
L10	1.5 x 10^3 ± 0.094	3.4 x 10^3 ± 0.033	2 nm	–18.12
L11	5.2 x 10^3 ± 0.042	4.4 x 10^3 ± 0.031	-	–21.20
L12	9.5 x 10^3 ± 0.032	3.4 x 10^3 ± 0.031	2 nm	–22.69
C17	1.8 x 10^4 ± 0.013	1.1 x 10^4 ± 0.037	2 nm	−24.28
C18	3.1 x 10^4 ± 0.021	4.4 x 10^3 ± 0.035	3 nm	−25.62
C19	6.7 x 10^4 ± 0.044	9.3 x 10^3 ± 0.039	-	−27.53
C20	5.7 x 10^3 ± 0.010	9.6 x 10^3 ± 0.036	3 nm	−21.43
C21	9.6 x 10^3 ± 0.018	4.6 x 10^4 ± 0.036	1 nm	−22.72
C22	2.8 x 10^4 ± 0.017	4.6 x 10^4 ± 0.031	2 nm	−25.37
C23	3.3 x 10^4 ± 0.034	5.0 x 10^4 ± 0.034	3 nm	−25.78
C24	2.4 x 10^4 ± 0.015	4.6 x 10^4 ± 0.051	-	–24.99

An overall view of the quenching constants suggest that the complexes **C17-24** are slightly more efficient in quenching the EB-DNA fluorescence as compared to the free ligands indicating their greater efficiency to replace EB and bind strongly with DNA which is also

evident from their higher K_b values. The nature of the bridging ligand (imidazole / 4, 4' azopyridine) apparently does not influence the mode or strength of DNA binding of the complexes. As mentioned earlier, viscosity measurement is often regarded as an effective and accurate method to determine the binding mode between complexes and DNA. The relative viscosities of CT-DNA solution increased gradually on the addition of increased amounts of the compounds *Fig. 4.10* (C) due to elongation of the double helix to accommodate the compounds within the base pairs thereby confirming intercalation.

4.2.4.4 *Ferrocenyl amino acid series*:

The absorption bands of all the complexes **C26-32** with ferrocene derivatized amino acids as ligands showed hypochormism and bathochromic shift. $\mathbf{K_b}$ values for the ligands **L13-16** are in the range of 1.3 – 6.7 x 10^4 M^{-1} indicative of moderate to strong binding of the ligands to CT-DNA with **L13** showing the highest value. It is observed that complexation of the ligands do not increase their binding efficacies in most of the cases. This may be due to the large size of the complexes which may partially hinder intercalation due to steric crowding as observed in the previous section. **C32** with tryptophan substituted ferrocenyl moieties bound to metal centres shows higher $\mathbf{K_b}$ values probably due to additional H-bonding interactions between –NH group of tryptophan and DNA nucleobases. The quenching constant $\mathbf{K_{SV}}$ values in the order of 10^3 M^{-1} for most of the complexes**,** obtained from Stern-Volmer quenching plots (*Fig. 4.9* G, H) also indicates moderate binding of the complexes to CT-DNA in agreement with the K_b values. Viscosity of DNA solutions was measured in the presence and absence of the complexes to confirm the mode of binding of the complexes to CT-DNA. The effects of addition of increasing amounts of **C25–32** and EB on the viscosity of CT-DNA solutions are shown in *Fig 4.10* (D). The increase in the relative viscosity of CT-DNA solutions with increase in the concentration as also observed for EB confirms the intercalative mode of binding of the complexes.

Table 4.4 : *DNA binding constants of* ***L13-16***, ***C25-28*** *and* ***C29-32***				
Code	***DNA binding constant***			
	$K_b\ M^{-1}$	$K_{SV}\ M^{-1}$	***λ shift***	**ΔG° kJmol^{-1}**
L13	6.7 x 10^4 ± 0.018	1.8 x 10^3 ± 0.049	2 nm	−27.53
L14	2.3 x 10^4 ± 0.058	1.2 x 10^3 ± 0.041	1 nm	−24.88
L15	1.4 x 10^4 ± 0.085	1.1 x 10^3 ± 0.036	3 nm	−23.63
L16	1.3 x 10^4 ± 0.074	1.3 x 10^3 ± 0.096	3 nm	−23.47
C25	5.5 x 10^3 ± 0.086	1.4 x 10^4 ± 0.075	2 nm	−21.34
C26	9.3 x 10^3 ± 0.014	6.3 x 10^3 ± 0.096	1nm	−22.64
C27	3.5 x 10^3 ± 0.017	8.6 x 10^3 ± 0.041	3 nm	−20.22
C28	8.6 x 10^3 ± 0.016	1.8 x 10^4 ± 0.048	1 nm	−22.44
C29	3.2 x 10^4 ± 0.049	1.5 x 10^4 ± 0.050	2 nm	−25.70
C30	7.0 x 10^4 ± 0.074	5.3 x 10^4 ± 0.064	1 nm	−27.64
C31	4.9 x 10^3 ± 0.086	6.8 x 10^3 ± 0.053	-	−21.05
C32	1.2 x 10^5 ± 0.063	1.1 x 10^5 ± 0.057	1 nm	−28.98

4.2.4.5 *Fluoroquinolone* series:

In case of the fluoroquinolones as secondary ligands, the binding constant K_b values (Table 4.5) as calculated from the plots in *Fig. 4.5* I, J are in the order of 10^3 M^{-1} for **L17-20** and 10^4-10^5 M^{-1} for **C33-C40.** All of the complexes are showing higher K_b values than the corresponding ligands **L17 – 20**. The higher K_b values of the complexes suggest ligation of the quinolones to the Ru (II) centres enhances their DNA binding efficacies due to the presence of additional cationic centres and enhanced hydrophobicity of the binuclear

complexes. It is observed that the complexes with moxifloxacin (**C36** and **C40**) and ciprofloxacin (**C39**) as ligands display higher DNA binding efficacy. This can be attributed to the presence of a cyclopropyl moiety at the N-1 position of these FQs. It has been reported that a cyclopropyl substituent on the N-1 position of the FQs facilitates hydrophobic interactions with the major grooves of DNA [72]. Competitive binding studies with EB, was employed by fluorescence experiments (*Fig. 4.7* I, J). The corresponding stern – volmer quenching constants $\boldsymbol{K_{SV}}$ (Table 4.5) obtained from the Io/I versus [Q] quenching plots (*Fig. 4.9* I, J) reveal moderate ($10^3 – 10^4\ M^{-1}$) to strong quenching of EB-DNA fluorescence.

Table 4.5 : *DNA binding constants of* ***L17-20***, ***C33-36*** *and* ***C37-40***

Code	***DNA binding constant***			
	$\boldsymbol{K_b\ M^{-1}}$	$\boldsymbol{K_{SV}\ M^{-1}}$	***λ shift***	**ΔG° kJmol^{-1}**
L17	4.7 x 10^3 ± 0.129	7.2 x 10^3 ± 0.175	-	−20.95
L18	7.8 x 10^3 ± 0.278	7.5 x 10^3 ± 0.044	-	−22.20
L19	7.2 x 10^3 ± 0.084	6.3 x 10^3 ± 0.091	-	−22.18
L20	1.6 x 10^3 ± 0.032	2.4 x 10^3 ± 0.178	-	−18.28
C33	1.2 x 10^5 ± 0.027	1.1 x 10^4 ± 0.048	3 nm	−29.06
C34	1.2 x 10^4 ± 0.019	5.8 x 10^3 ± 0.038	-	−23.27
C35	1.4 x 10^4 ± 0.024	7.7 x 10^3 ± 0.069	2 nm	−23.47
C36	2.4 x 10^5 ± 0.052	1.8 x 10^4 ± 0.060	1 nm	−30.69
C37	2.3 x 10^4 ± 0.044	3.4 x 10^3 ± 0.085	-	−24.88
C38	7.0 x 10^4 ± 0.023	1.2 x 10^4 ± 0.032	-	−27.64
C39	1.9 x 10^5 ± 0.047	5.6 x 10^4 ± 0.074	1 nm	−29.46
C40	1.8 x 10^5 ± 0.088	4.5 x 10^4 ± 0.056	2nm	−29.98

Viscosity measurements of DNA solutions in the presence and absence of the complexes (*Fig. 4.10* E) showed a decrease in viscosity with increased concentrations of the complexes, further confirming the intercalative mode of binding of the complexes.

4.3 BSA interactions:

Large number of biomolecules are encountered in living organisms; from a functional point of view, proteins are the most abundant and diverse form. Starting from the hormones and enzymes, known to control metabolism, the collagen in bones, the contractile proteins in muscles, as well as the haemoglobin and albumin in the bloodstream and immunoglobulins, almost every life process is dependent on this class of biomolecules. Serum albumins are the most soluble proteins found in mammalian blood plasma (about 60% of the total protein content of plasma) that have many physiological functions and play an vital role in the transportation, distribution and metabolism of many drug molecules, amino acids, fatty acids, and metal ions [73]. In order to understand the pharmacodynamics and pharmacokinetics of drugs, the investigation of the binding amplitude and mechanism of interaction of small molecules with serum albumins is very important, as the nature and strength of their interaction has a great influence on drug absorption, metabolism, excretion and distribution [74, 75]. Bovine serum albumin (BSA) is usually selected as a relevant model when approaching towards the evaluation of small molecules affinity for albumins, due to its low cost, wide availability and most importantly its ~76% structural similarity with human serum albumin (HSA) [76, 77].

4.3.1 Bovine serum albumin structure and biological functions:

The BSA molecule is made up of 583 amino acids, which are bound in a single chain and are cross-linked with 17 cystine residues (eight disulfide bonds and one free thiol group), with a molecular mass of 66400 Da [78]. The amino acid chain is consisting of three homologous but structurally distinct domains (I, II and III), which are further divided into nine loops by the disulfide bonds and are arranged in a heart-shaped molecule. Each domain is further separated into two sub-domains, A and B. The secondary structure of the protein is mainly α-helical (74%), with the remaining polypeptide chain occurring in turns and in extended or flexible regions between sub-domains [79, 80]. BSA is a globular non-glycosylated protein. BSA is synthesized in the liver lacking prosthetic groups, carbohydrate group or other additives. One of the most important characteristic structural features of BSA is that it

content very low tryptophan, methionine, glycine and isoleucine, while rich in an ionic amino acids, such as glutamic acid and lysine. The ionized residues confer the protein a high total charge, of 185 ions per molecule at neutral pH, contributing to its solubility [78].

Many drugs, hormones, xenobiotics and fatty acids [81], form a complex with serum albumins once they entered the blood stream, are transported and disposed. This class of proteins also contribute to the colloid blood osmotic pressure and helps in maintaining blood pH [82, 83], but one of the most important characteristic of albumins is that they reversibly bind to different compounds in different manner. The protein often influences the circulation, metabolism and efficacy of hydrophobic drugs in the plasma by increasing their solubility [76, 78].

BSA shows very specific binding sites, of which most important one being referred is site-I and site-II, located in hydrophobic cavities of sub-domains IIA and IIIA respectively [78] as shown in *Fig. 4.11*. Site markers are small molecules, often used in studying the interaction of different ligands with the protein as they have specific binding locations in the albumin structure.

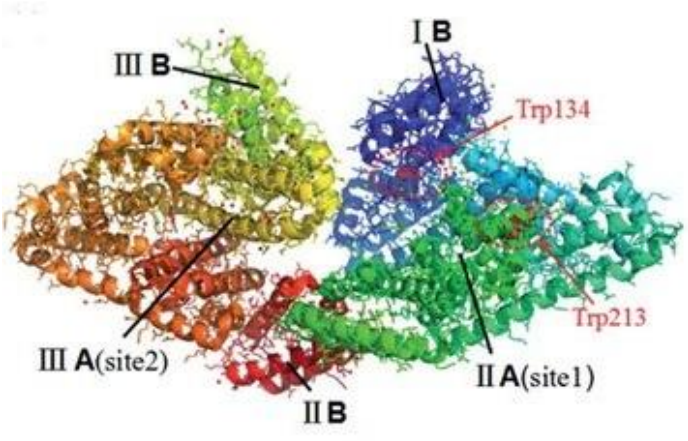

Fig. 4.11: *Discrete binding sites of BSA*

4.3.1.1 Fluorescence property of BSA and type of interaction:

BSA has fluorescent properties and emits intensely upon excitation. The intrinsic fluorescence in the BSA is due to the presence of three amino acid residues: tryptophan, tyrosine and phenylalanine [78], but as the relative ratio of fluorescence intensity for these amino acids is 100: 9: 0.5, it seems probable that the fluorescence of BSA arises mainly from its two tryptophan residues: Trp- 134 located on the surface of sub-domain IB and Trp-212 located within a hydrophobic binding pocket in sub-domain IIA [84, 85]. The Trp and Tyr

residues in serum albumin are excited at 280 nm wavelength, whereas at 295 nm wavelength only Trp residues are excited. Interactions between small molecules like metal complexes and BSA are usually affirmed when the fluorescence intensity of the protein around 345 nm decreases regularly with the increase in concentration of the probe. Moreover, a red or blue shift of the emission maximum in the fluorescence spectrum of the albumin is indicative of an increase in the hydrophobicity of the microenvironment around the tryptophan residues [86]. Fluorescence quenching can occur by different mechanisms, usually classified as static quenching (a non-fluorescent ground-state complex is formed between the fluorophore and the quencher), dynamic quenching (a collisional process, the fluorophore and the quencher interact during the transient existence of the excited state), or a simultaneous static and dynamic quenching [77].

A linear I_0/I *vs.* [Q] plot obtained using Stern – Volmer equation (where Io and I are the emission intensities in the absence and the presence of the quencher Q), indicates which type of quenching mechanism is involved, either static or dynamic, while a deviation from linearity suggests a mixed quenching mechanism [87]. Dynamic and static quenching show certain characteristics, such as their different dependence on temperature reflected in the changes in the fluorescence spectrum of the fluorophore. In the case of static quenching, an increase in temperature leads to a lower stability of the complex and a decrease in the quenching constant. In the case of dynamic quenching, a faster diffusion is a consequence of an increase in temperature and, thus, the quenching rate increases [77, 88]. A static quenching, consequence of a new species formed between the quencher and the ground-state of the fluorophore, leads to considerable changes in the absorption spectra at 280 nm (either a red or a blue shift, bathochromism or hypsochromism respectively). In the case of dynamic quenching, the absorption spectra suffer no modifications, as only the excited-state fluorescent molecule interacts with the quencher [83].

4.3.1.2 Metal complexes interacting with BSA

An interaction between BSA and metal complexes often leads to a perturbation of the secondary structure of the protein, by disrupting the disulfide bonds and leading to a partial loss of α-helix conformation with the subsequent unfolding of the protein [88], or a change in the polarity of the environment to which the tryptophan residues are exposed [84], as a result of molecular interactions, such as excited-state reactions, molecular rearrangements, energy transfer, ground-state complex formation or collision quenching [80].

The BSA interaction and binding ability of a large variety of mononuclear and polynuclear Cu^{2+}, Ni^{2+}, Zn^{2+}, Co^{2+}, Pt^{2+} complexes with aromatic ligands (some of them bearing known pharmacologically active moieties) has been investigated [88]. As in the case of the interaction of metal complexes with other classes of biomolecules, it has been suggested that the planarity of the ligands coordinating the metal centre plays an important role in enhancing protein binding ability [89]. A certain degree of binding specificity was observed for metal complexes, due to weak interactions between the ligand sphere and the protein binding site, as some studies suggested that metal complexes most likely affect the Trp134 residue, found on the surface of the protein, and thus more accessible [90]. Other research groups, after performing displacement experiments, concluded that complexes preferentially bind to subdomain IIA (site-I) [91]. Site-I markers include warfarin, phenylbutazone, dansylamide and iodipamide, while site-II markers include ibuprofen, flufenamic acid and diazepam as shown in *Fig. 4.12* [92].

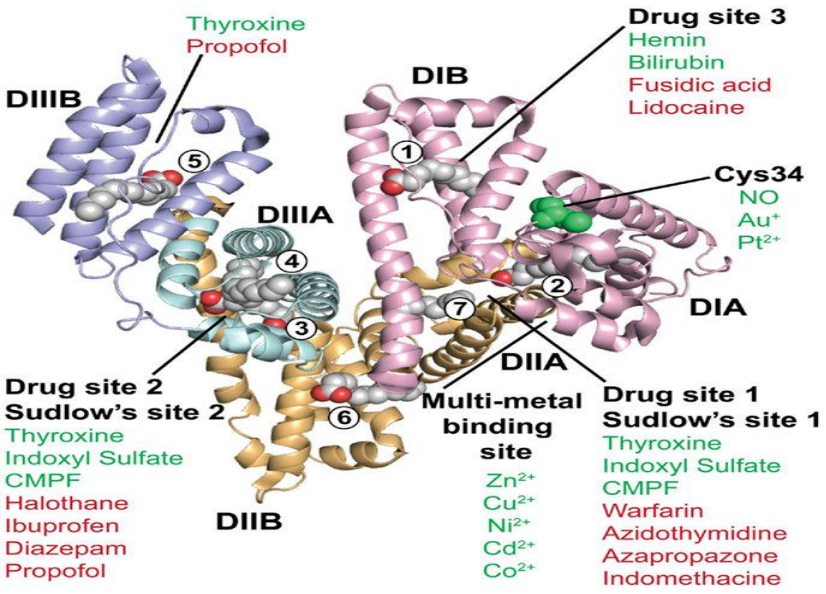

Fig. 4.12: *Binding sites available for metals and drugs*

Ruthenium complexes of S-Allyl-L-cysteine sulfoxide (alliin) were found to show considerable affinity to bind BSA. Complexes quench the fluorescence of the protein by static mechanism hence forming complex – protein adduct in the ground state. The nature of the binding forces between complexes and BSA was observed to be related to the coordination mode of alliin. Complexes having O-bound alliin predominantly interact with BSA through hydrogen bonding and van der Waals interactions, while the hydrophobic forces govern the interaction of species having ionized carboxylate group [93].

4.3.2 Materials and instrumentation:

The BSA (Bovine Serum Albumin) binding studies were carried out in tris buffer. BSA stock solution was prepared in double distilled water with a concentration of 10^{-4} M. The stock solutions of all the compounds under study were prepared in DMSO with a stock concentration of 10^{-3} M. BSA was purchased from Hi-media, Mumbai, India. Fluorescence spectra were recorded on JASCO FP-6300 fluorescence spectrophotometer. The data generated from the titration experiments were analysed and plotted with the help of the software OriginPro 8.

4.3.3 Experimental:

The protein-binding study was performed employing steady state fluorescence spectroscopy. Tryptophan fluorescence quenching experiments were carried out using bovine serum albumin (BSA, 16.6 μM) in buffer (containing 15 mM trisodium citrate and 150 mM NaCl at pH 7.0). The stock solution of complexes (10^{-3}M) was prepared in DMSO and diluted with buffer. The test solutions contained no more than 1% DMSO. BSA solutions exhibit a strong fluorescence emission with a peak at 343 nm, due to the tryptophan residues, when excited at 296 nm, as a result the peak at 343 nm was monitored during experiment [94]. In the fluorescence quenching experiments, a 100μL of BSA (16.6 μM) and 2900μL of buffer was placed in a quartz cuvette, total volume in the cuvette was 3000μL and the corresponding peak was observed at 343 nm. Further the titration was carried out with 5μL increasing concentrations of the complexes (0 – 25 μM) as quenchers. The titration curves so generated have been representatively shown in *Fig. 4.12* and *4.13*.

$$\mathbf{Io/I = 1 + K_{SV}\,[Q] = 1 + k_q\tau_0[Q]} \qquad \mathbf{(4.3)}$$

where Io is the initial tryptophan fluorescence intensity of BSA, I is the tryptophan fluorescence intensity of BSA after the addition of the quencher and $\boldsymbol{K_{SV}}$ the dynamic quenching constant, [Q] is the concentration of the quencher, kq is the quenching rate constant of the biomolecule and τ0 is the average lifetime of the molecule in the absence of the quencher. The dynamic quenching constant ($\boldsymbol{K_{SV}}$ M^{-1}) can be obtained from the slope of the plot Io/I *versus* [Q]. The $\boldsymbol{K_{SV}}$ plots for all the synthesized ligands and their corresponding binuclear Ru(II) complexes have been shown in *Fig. 4.15* and *4.16*. The $\boldsymbol{K_{SV}}$ values obtained from these plots have been tabulated and discussed in section 4.3.4.

Binding of small molecules to a set of equivalent sites on the protein results into equilibrium between the free and bound molecules represented by the double logarithm equation **(4.4)** [95]. This equation has been employed in order to determine the binding constant (***Ka***) and the number of binding sites (***n***) for complex – BSA interaction.

$$\textbf{Log (Io-I)/I = log } K_b \textbf{ + } n \textbf{ log [Q]} \qquad \textbf{(4.4)}$$

where Io and I are the fluorescence intensities in the absence and the presence of quencher, and [Q] is the concentration of quencher (binuclear ruthenium complexes).The plot of log [(Io-I)/I] *versus* log [Q] for all the systems is linear (*Fig 4.17* and *4.18*) and the values of $\mathbf{K_a}$ (M^{-1}) and ***n*** have been obtained from the intercept and slope, respectively.

.

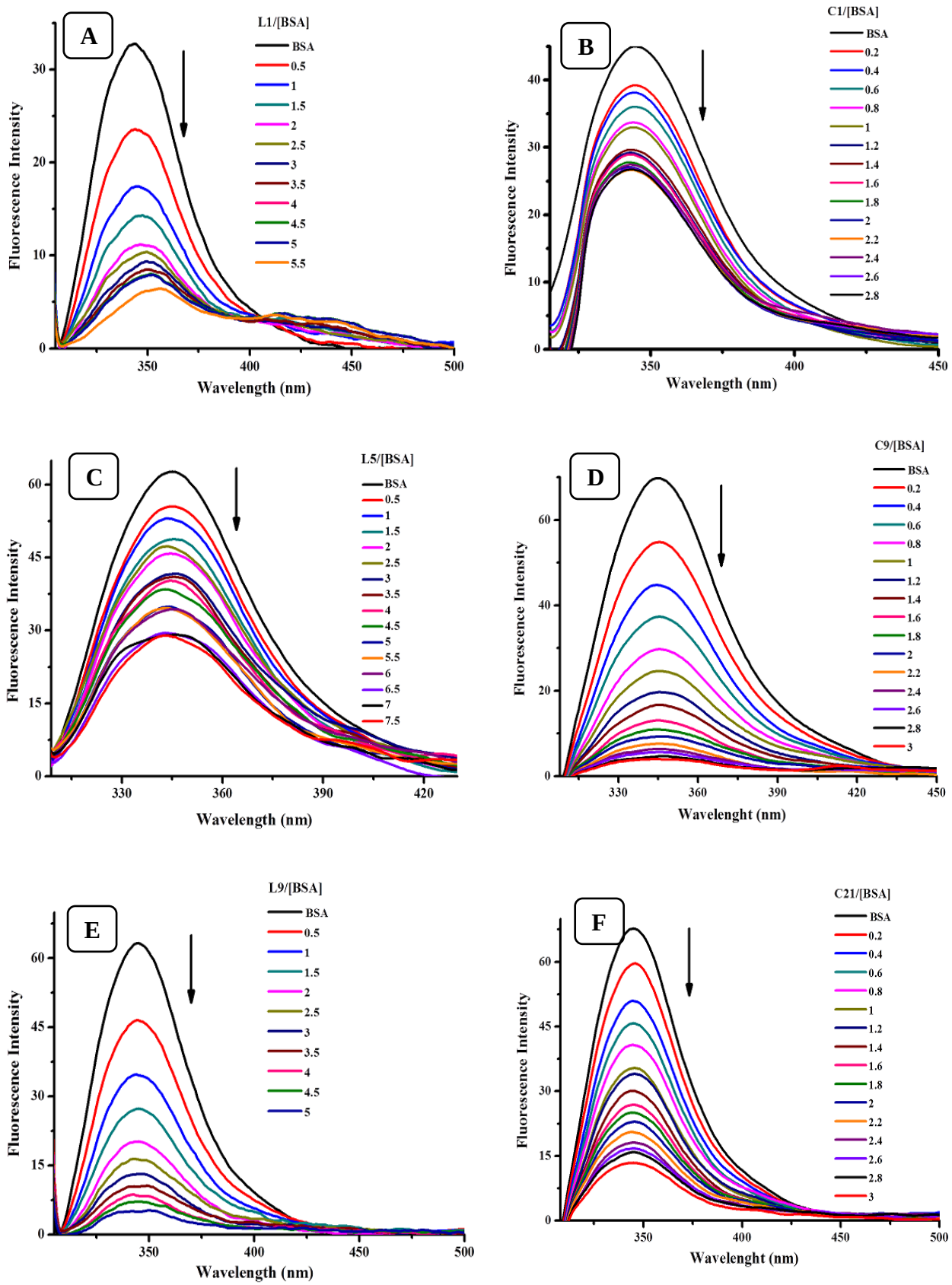

Fig. 4.13: *Fluorescence emission spectra of BSA at increasing concentrations of (A)* ***L1*** *(B)* ***C1*** *(C)* ***L5*** *(D)* ***C9*** *(E)* ***L9*** and *(F)* ***C21*** *the arrow shows decrease in intensity (quenching of BSA fluorescence) upon increasing concentration of the complex.*

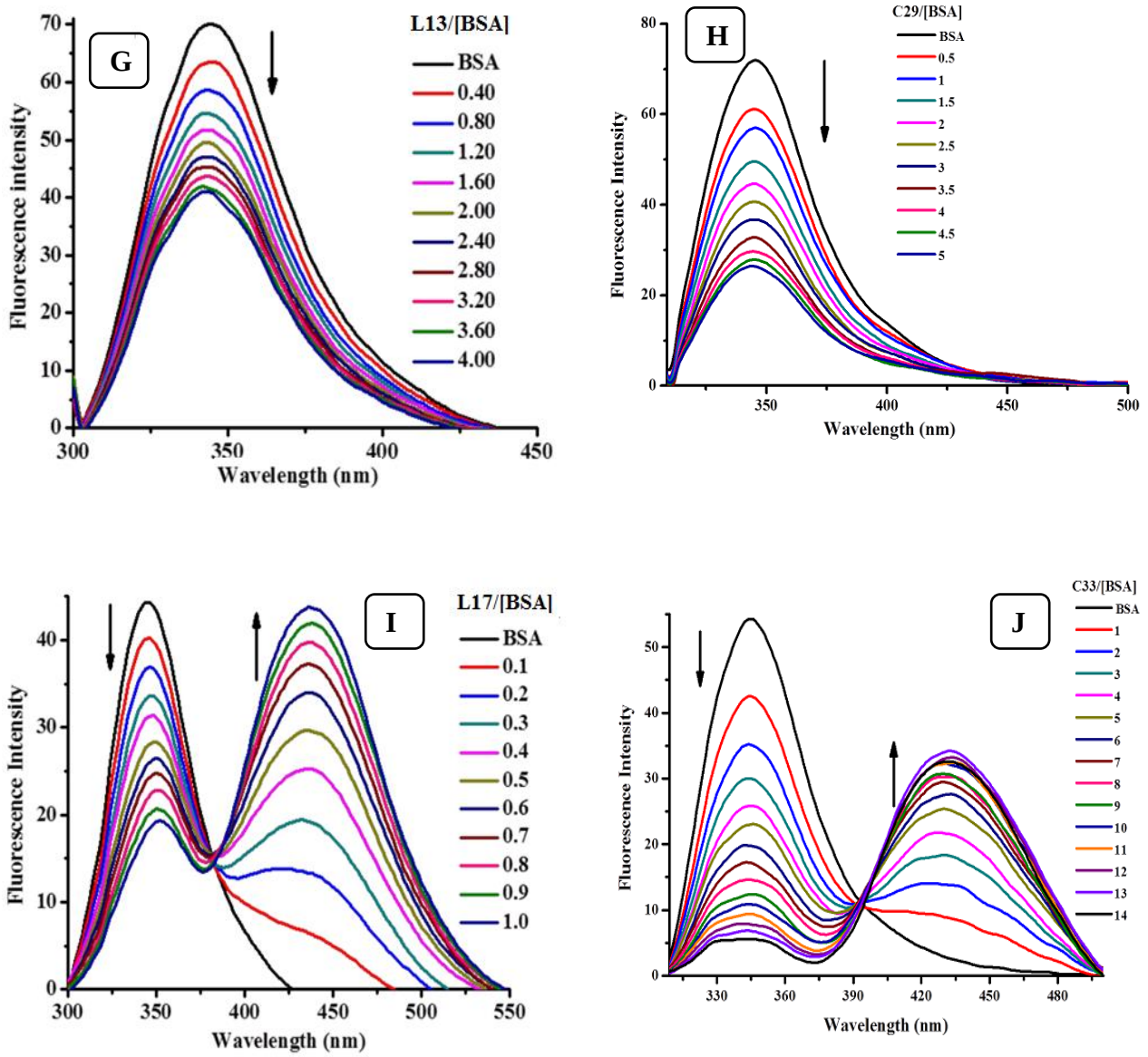

Fig. 4.14 (Cont...): *Fluorescence emission spectra of BSA at increasing concentrations of (G)* ***L13*** *(H)* ***C29*** *(I)* ***L17*** and *(J)* ***C33*** *the arrow shows decrease in intensity (quenching of BSA fluorescence) upon increasing concentration of the compounds*

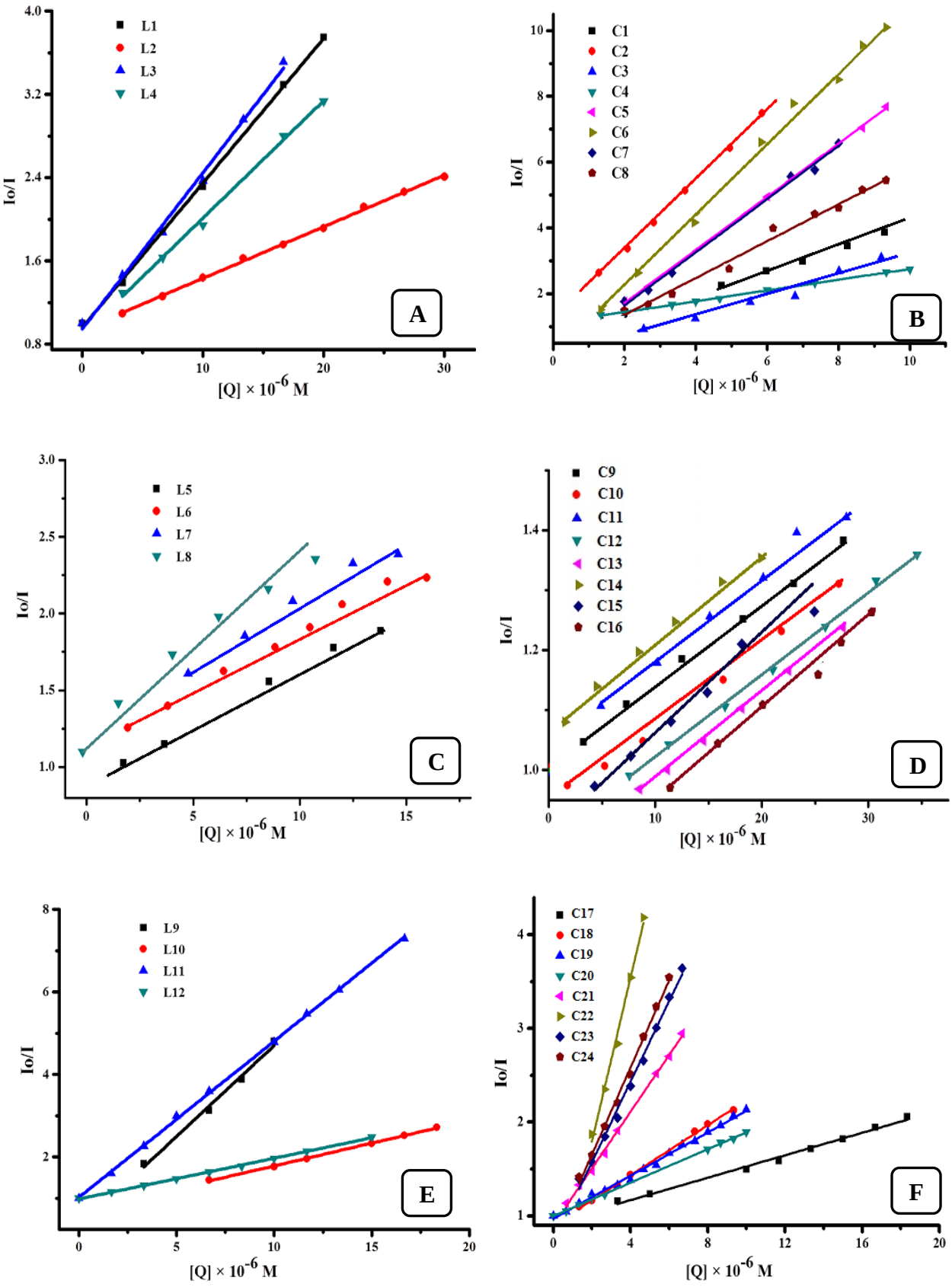

Fig. 4.15: *Stern-Volmer quenching plot Io/I versus [Q] of BSA for (A)* ***L1-4*** *(B)* ***C1-8*** *(C)* ***L5-8*** *(D)* ***C9-16*** *(E)* ***L9-12*** and *(F)* ***C17-24***

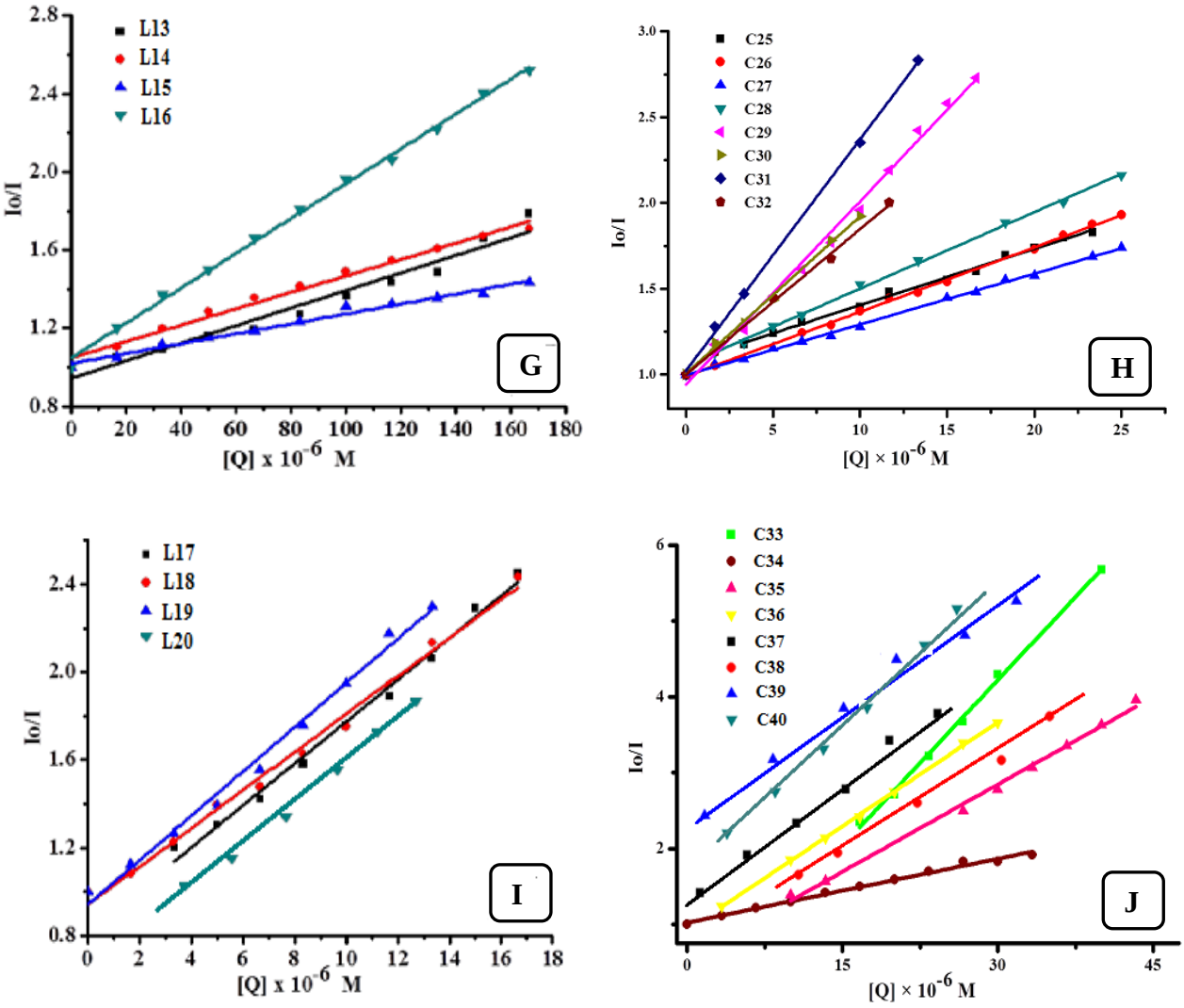

Fig. 4.16 (Cont...): *Stern-Volmer quenching plot Io/I versus [Q] of BSA for (G)* ***L13-16*** *(H)* ***C25-32*** *(I)* ***L17-20*** and *(J)* ***C33-40***

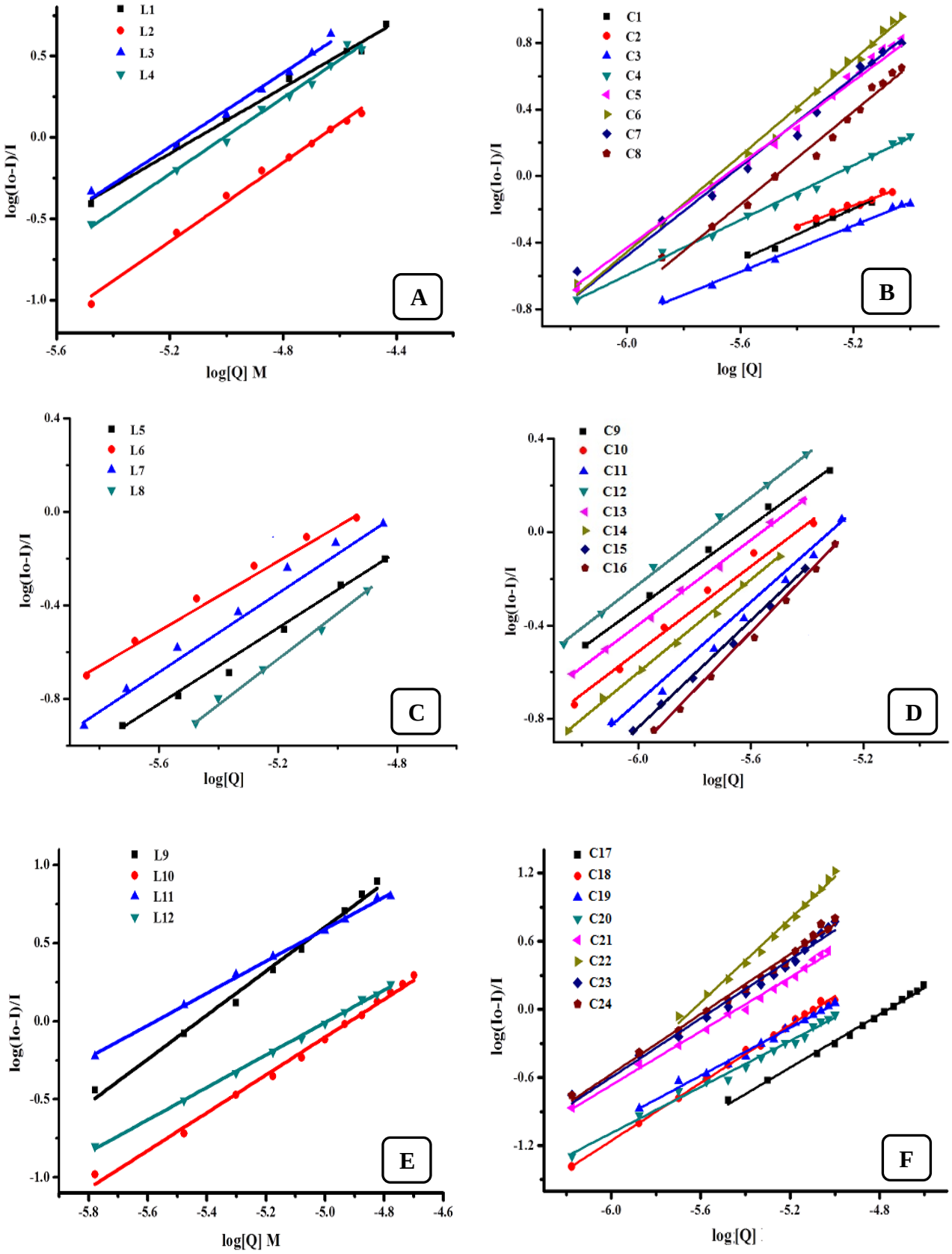

Fig. 4.17: *Double logarithmic plot for the quenching of BSA fluorescence by (A)* ***L1-4*** *(B)* ***C1-8*** *(C)* ***L5-8*** *(D)* ***C9-16*** *(E)* ***L9-12*** and *(F)* ***C17-24***

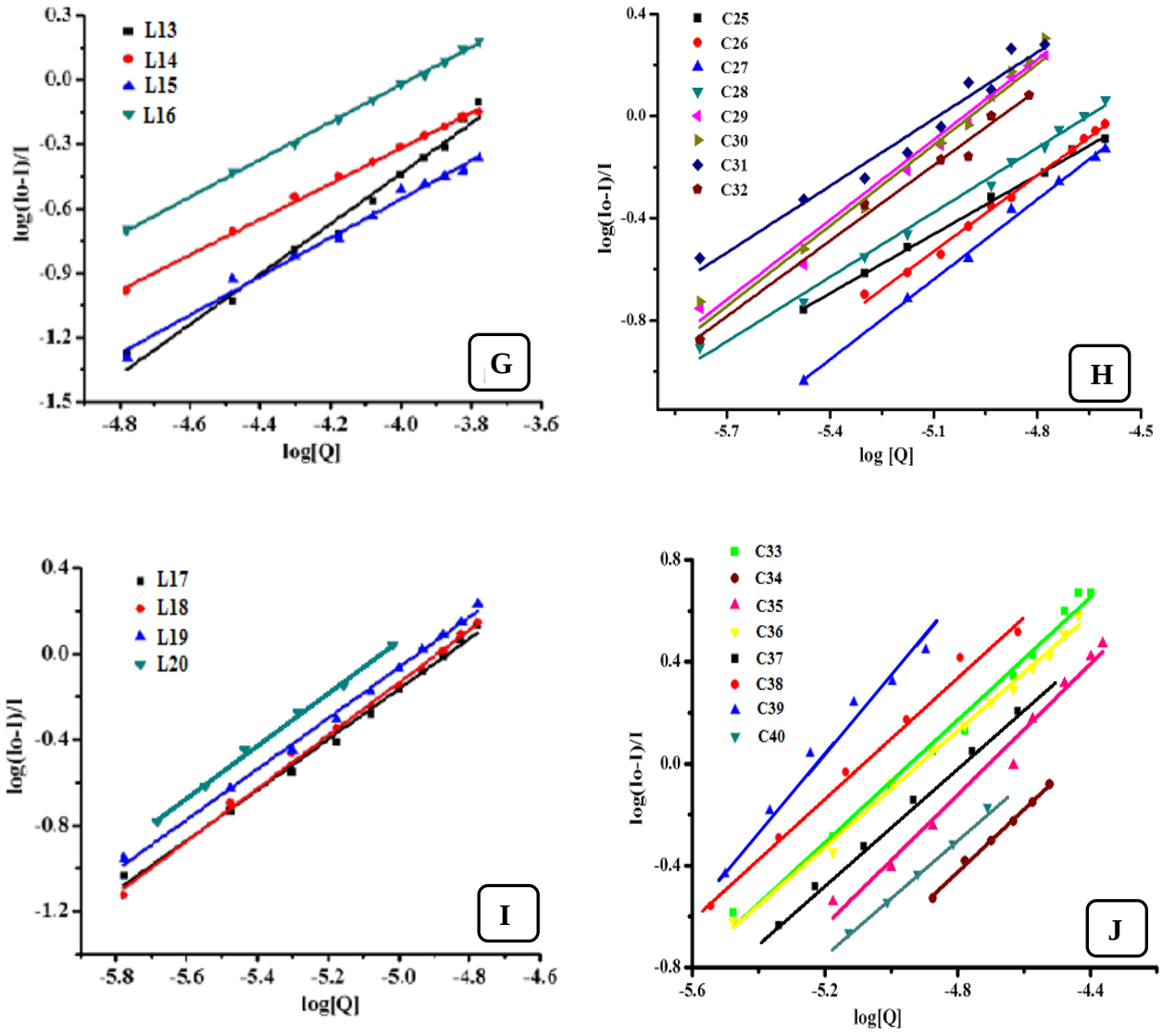

Fig. 4.18 (Cont...): *Double logarithmic plot for the quenching of BSA fluorescence by (G)* ***L13-16*** *(H)* ***C25-32*** *(I)* ***L17-20*** and *(J)* ***C33-40***

4.3.4 Results and discussion

The binding interactions of all the ligands/complexes under study with BSA led to quenching of its fluorescence.

4.3.4.1 *Diphenyl pyrazol thiosemicarbazones Series:*

The Stern–Volmer plots (*Fig. 4.15 A,B*) show that the curves have linear relationships (R= 0.98) according to the Stern–Volmer quenching equation **(4.3)** indicative of a single quenching (static or dynamic) process in the system**.** The Stern-Volmer quenching constant K_{SV} values for the ligands as well as complexes are in the order of 10^4-$10^5 M^{-1}$ (*Table 4.6*).

Table 4.6 : *BSA binding constants of* ***L1-4***, ***C1-4*** *and* ***C5-8***

Code	***BSA binding constant***			
	$K_a\ M^{-1}$	$K_{SV}\ M^{-1}$	***n***	ΔG° $kJmol^{-1}$
L1	$6.7 \times 10^3 \pm 0.206$	$9.1 \times 10^4 \pm 0.085$	1.0	−21.83
L2	$1.2 \times 10^3 \pm 0.205$	$7.7 \times 10^4 \pm 0.053$	1.0	−17.56
L3	$2.0 \times 10^3 \pm 0.202$	$6.4 \times 10^4 \pm 0.099$	1.1	−18.83
L4	$2.3 \times 10^4 \pm 0.205$	$2.2 \times 10^5 \pm 0.078$	0.8	−24.88
C1	$1.5 \times 10^5 \pm 0.187$	$1.4 \times 10^5 \pm 0.235$	1.0	−29.53
C2	$1.1 \times 10^6 \pm 0.191$	$9.9 \times 10^4 \pm 0.173$	1.2	−34.47
C3	$7.1 \times 10^5 \pm 0.186$	$1.5 \times 10^5 \pm 0.208$	1.1	−33.38
C4	$1.6 \times 10^6 \pm 0.184$	$1.6 \times 10^5 \pm 0.164$	1.2	−35.39
C5	$3.6 \times 10^5 \pm 0.185$	$8.1 \times 10^5 \pm 0.154$	1.3	−31.70
C6	$1.6 \times 10^5 \pm 0.185$	$1.0 \times 10^4 \pm 0.148$	1.4	−29.69
C7	$1.2 \times 10^6 \pm 0.183$	$8.1 \times 10^5 \pm 0.180$	1.2	−34.68
C8	$4.3 \times 10^6 \pm 0.187$	$5.6 \times 10^5 \pm 0.152$	1.3	−37.84

This indicates strong interaction with the protein. The K_{SV} values reveal that the complexes are more efficient in quenching the fluorescence of BSA compared to the ligands due to increased hydrophobicity. Quantitative binding to BSA was achieved using double logarithmic plot. The plots of log [(Io-I)/I] *versus* log [Q] are linear (*Fig. 4.17 A, B*) and the values of association constant K_a and number of binding sites on BSA ***n*** have been tabulated in *Table 4.6.* The K_a values for the complexes are within the range of 10^4–10^6 M^{-1} as expected from a good BSA carrier activity *in vivo* [96].

The *n* values for the ligands and the complexes average out to be 1.0 which suggests that there is one binding site available for the compounds on the protein. Moreover the linear nature of the double logarithm plots of the complexes also indicates that only one of the tryptophan residues on BSA protein is interacting with the compounds.

4.3.4.2 *Diphenylpyrazol α-Amino acid derivatives series:*

The K_{SV} values obtained from Stern-Volmer plot I_0/I *vs.* [Q] (*Fig. 4.15* C, D) and the K_a values obtained from double logarithm plot log[$(I_0-I)/I$] *vs.* log[Q]. (*Fig. 4.17* C, D) for the interaction of diphenylpyrazol α-amino acid derivatives and their binuclear ruthenium complexes with BSA given in Table 4.7 suggest moderate to strong binding efficacies. It is observed that the protein binding of the ligands (K_a ~ 10^3 – 10^4 M^{-1}) is improved upon coordination. The K_a values of the complexes **C9–16** in the range of 10^4–10^5 M^{-1} is indicative of an efficient interaction with the protein [75, 77, 83]. Generally, the binding constant of a compound to serum albumin should be high enough to ensure that a significant amount gets transported and distributed through the organism, but, at the same time, low enough so that the compound can be released once it reaches its target this optimum range is 10^4–10^6 M^{-1} [97, 98]. In addition **C10** (K_a = 3.9 x 10^5 M^{-1}) and **C14** (K_a =7.1 x 10^5 M^{-1}) displayed slightly better binding affinity amongst all the other complexes. The number of binding sites ***n*** ≈ 1 values suggests that there is one site available on the protein for binding. The double logarithm equation 4.3 as discussed in section 4.3.3 represents equilibrium between the free and bound molecules. Moreover the linear nature of the double logarithm plots indicates one of the tryptophan residues on BSA is interacting with the compounds [89].

Table 4.7 : *BSA binding constants of* ***L5-8***, ***C9-12*** *and* ***C13-16***				
Code	***BSA binding constant***			
	$K_a\ M^{-1}$	$K_{SV}\ M^{-1}$	***n***	**ΔG° kJmol^{-1}**
L5	4.8 x 10^3 ± 0.145	1.2 x 10^3 ± 0.126	1.0	−21.00
L6	2.8 x 10^4 ± 0.024	7.2 x 10^3 ± 0.089	0.9	−25.37
L7	7.3 x 10^3 ± 0.102	3.3 x 10^4 ± 0.045	0.8	−22.04
L8	1.7 x 10^3 ± 0.089	1.4 x 10^4 ± 0.022	0.9	−18.43
C9	1.4 x 10^4 ± 0.134	2.1 x 10^4 ± 0.059	1.0	−23.65
C10	3.9 x 10^5 ± 0.256	5.6 x 10^4 ± 0.026	1.1	−31.90
C11	1.3 x 10^4 ± 0.378	7.6 x 10^4 ± 0.011	1.0	−23.47
C12	2.3 x 10^4 ± 0.024	1.7 x 10^4 ± 0.148	1.0	−24.88
C13	2.6 x 10^4 ± 0.015	3.4 x 10^4 ± 0.131	1.3	−25.19
C14	7.1 x 10^5 ± 0.068	1.2 x 10^5 ± 0.031	1.1	−33.38
C15	1.5 x 10^4 ± 0.128	5.6 x 10^4 ± 0.068	1.2	−23.82
C16	1.7 x 10^4 ± 0.147	4.5 x 10^5 ± 0.023	1.3	−24.13

4.3.4.3 *Ferrocenyl thiosemicarbazones series:*

The $\mathbf{K_a}$ and $\mathbf{K_{SV}}$ values (Table 4.8) of the synthesized ferrocenyl thiosemicarbazones and their binuclear Ru(II)-arene complexes interacting with BSA obtained from Stern-Volmer plots (*Fig. 4.15* E,F) and linear double logarithmic plots (*Fig. 4.17* E,F), suggest good binding propensity of the compounds with the serum protein. The $\mathbf{K_{SV}}$ values for complexes **C17-20** are in the order of and 10^4–10^5 M^{-1} whereas those for **C21-24** are in the order of 10^5 M^{-1} respectively indicating efficient fluorescence quenching of the trp residue of BSA due to protein-complex interactions leading to changes in its microenvironment. The association binding constant $\mathbf{K_a}$ values in the order of 10^5–10^7 M^{-1} for the complexes are comparable to

the binding constants of some biologically active molecules and anticancer drugs indicating efficient interaction with the protein for getting transported and distributed through the organism, but also released once it reaches its target [99]. The ***n*** values in the range of 1.0 – 1.3 confirm the existence of just one main binding site on BSA for the compounds.

Table 4.8 : *BSA binding constants of* ***L9-12***, ***C17-20*** *and* ***C21-24***

Code	***BSA binding constant***			
	$K_a\ M^{-1}$	$K_{SV}\ M^{-1}$	***n***	ΔG° $kJmol^{-1}$
L9	$1.6 \times 10^5 \pm 0.193$	$2.2 \times 10^5 \pm 0.133$	1.1	−29.69
L10	$8.8 \times 10^5 \pm 0.197$	$1.1 \times 10^5 \pm 0.073$	1.2	−33.91
L11	$2.6 \times 10^5 \pm 0.193$	$1.8 \times 10^5 \pm 0.107$	1.0	−30.89
L12	$1.5 \times 10^5 \pm 0.194$	$9.8 \times 10^4 \pm 0.120$	1.0	−29.53
C17	$3.6 \times 10^5 \pm 0.204$	$6.0 \times 10^4 \pm 0.078$	1.1	−31.70
C18	$3.0 \times 10^6 \pm 0.185$	$1.3 \times 10^5 \pm 0.181$	1.2	−36.95
C19	$2.0 \times 10^5 \pm 0.188$	$1.1 \times 10^5 \pm 0.170$	1.0	−30.24
C20	$1.0 \times 10^5 \pm 0.185$	$8.9 \times 10^4 \pm 0.162$	1.0	−28.52
C21	$2.8 \times 10^6 \pm 0.184$	$3.0 \times 10^5 \pm 0.244$	1.2	−36.78
C22	$2.3 \times 10^7 \pm 0.189$	$8.7 \times 10^5 \pm 0.288$	1.3	−42.00
C23	$1.4 \times 10^7 \pm 0.185$	$4.3 \times 10^5 \pm 0.229$	1.2	−40.77
C24	$2.3 \times 10^7 \pm 0.185$	$4.6 \times 10^5 \pm 0.251$	1.3	−42.00

4.3.4.4 *Ferrocene mannich bases series:*

The K_a and K_{SV} values in the order of $10^3 M^{-1}$ for the ligands and 10^4-10^5 M^{-1} for the complexes (Table 4.9) indicate moderate binding of the ligands and strong binding of the complexes. The Stern-Volmer plots and the linear double logarithmic plots have been

provided in *Fig. 4.16* G, H and *4.18* G, H respectively. Only one binding site is available on the BSA, mostly the Trp-212 residue as revealed by the ***n*** values in the range of 0.8 – 1.1. The linear nature of the double logarithm plots further supported the interaction between the tryptophan residues on BSA protein and the ligands/complexes [100]. The binding efficacies of the azopyridine bridged complexes **C29-32** appear to be about 10-100 fold better than that of the imidazole bridged complexes **C25-28** which has also been observed in some of the earlier series.

Table 4.9 : *BSA binding constants of* ***L13-16***, ***C25-28*** *and* ***C29-32***

Code	***BSA binding constant***			
	$K_a\ M^{-1}$	$K_{SV}\ M^{-1}$	***n***	ΔG° $kJmol^{-1}$
L13	$1.8 \times 10^3 \pm 0.074$	$4.5 \times 10^3 \pm 0.023$	0.9	−18.57
L14	$1.0 \times 10^3 \pm 0.018$	$4.2 \times 10^3 \pm 0.027$	0.8	−17.11
L15	$1.1 \times 10^3 \pm 0.021$	$2.5 \times 10^3 \pm 0.038$	0.9	−17.35
L16	$3.0 \times 10^3 \pm 0.048$	$8.9 \times 10^3 \pm 0.071$	0.9	−19.83
C25	$2.9 \times 10^3 \pm 0.200$	$3.3 \times 10^4 \pm 0.065$	0.8	−19.75
C26	$3.4 \times 10^4 \pm 0.204$	$3.7 \times 10^4 \pm 0.065$	1.0	−25.85
C27	$4.8 \times 10^4 \pm 0.202$	$2.9 \times 10^4 \pm 0.069$	1.0	−26.71
C28	$8.4 \times 10^3 \pm 0.198$	$4.5 \times 10^4 \pm 0.070$	0.8	−22.39
C29	$1.8 \times 10^5 \pm 0.194$	$1.1 \times 10^5 \pm 0.101$	1.1	−29.98
C30	$1.2 \times 10^5 \pm 0.195$	$9.1 \times 10^4 \pm 0.170$	1.1	−28.98
C31	$2.7 \times 10^4 \pm 0.193$	$1.3 \times 10^5 \pm 0.131$	0.8	−25.28
C32	$6.8 \times 10^4 \pm 0.193$	$8.4 \times 10^4 \pm 0.146$	0.9	−27.57

4.3.4.5 *Fluoroquinolone series:*

Fig 4.14 I, J show the decrease in the emission intensity of BSA upon addition of increasing amounts of the fluroquinolones (**L13-16**) and their complexes (**C33-40**). The fluorescence intensity of the BSA solution at around 345 nm decreases regularly as the concentration of the compounds increase due to interactions while an additional peak observed at ~ 438 nm for the ligands and at ~ 432 nm for the complexes owing to the intrinsic fluorescence of the compounds exhibit hyperchromism with increased concentrations as expected.

Table 4.10 : *BSA binding constants of* ***L17-20, C33-C40***

Code	***BSA binding constant***			
	$K_a\ M^{-1}$	$K_{SV}\ M^{-1}$	***n***	ΔG° $kJmol^{-1}$
L17	5.3 x 10^4 ± 0.073	6.5 x 10^4 ± 0.125	1.1	−26.95
L18	1.1 x 10^5 ± 0.081	8.6 x 10^4 ± 0.015	1.2	−28.76
L19	2.2 x 10^4 ± 0.043	1.0 x 10^4 ± 0.165	1.1	−24.67
L20	1.3 x 10^4 ± 0.017	2.4 x 10^5 ± 0.084	0.9	−23.47
C33	8.8 x 10^5 ± 0.208	1.1 x 10^5 ± 0.036	1.2	−33.91
C34	1.9 x 10^5 ± 0.213	1.4 x 10^5 ± 0.050	1.1	−30.12
C35	2.7 x 10^6 ± 0.212	1.4 x 10^5 ± 0.032	1.3	−36.69
C36	8.8 x 10^5 ± 0.208	1.8 x 10^5 ± 0.052	1.1	−33.91
C37	1.2 x 10^6 ± 0.185	4.1 x 10^5 ± 0.257	1.3	−34.68
C38	3.1 x 10^6 ± 0.182	8.0 x 10^5 ± 0.557	1.0	−37.03
C39	1.1 x 10^5 ± 0.179	2.2 x 10^5 ± 0.307	0.9	−28.76
C40	1.6 x 10^5 ± 0.180	4.1 x 10^5 ± 0.442	1.1	−29.69

The association binding constant K_a (Table 4.10) so calculated indicate that the complexes **C33-40** with Ka values in the range of 1.1 x 10^5 - 3.1 x 10^6 M^{-1} interact with the protein 10-100 folds better than the ligands **L13-16** with K_a values in the range of 1.3 x 10^4 - 1.1 x 10^5 M^{-1}. The values of the Stern–Volmer quenching constant (K_{SV}) obtained from the plot of [Io/I] versus [Q] for the complexes interacting with BSA are in the order of 10^5 M^{-1} which also suggest strong binding propensity of the complexes to BSA probably due to the presence of two hydrophobic arene moieties which can interact strongly with the hydrophobic groups of the amino acid residues. The plot of log [(Io-I)/I] versus log [Q] for all the complexes is linear (*Fig. 4.18* I, J). The association binding constant (K_a M^{-1}), and the number of binding sites per albumin (*n*) have been obtained from the intercept and slope, respectively. The K_a values in the order of 10^6 M^{-1} also indicate strong binding of the complexes to BSA in agreement to the K_{sv} values. The *n* values around ~1 and linearity of plot suggested interaction between one of the tryptophan residues BSA and the compounds.

In-Cellulo assays

4.4 Cytotoxicity on HeLa (human cervical cancer) cell lines:

Cancer is one of humanity's greatest health challenges today as it is the second leading cause of death globally behind cardiovascular diseases, accounting for the deaths of more than 9.6 million people from an estimated 18.1 million cancer cases around the world in 2018, with 9.5 million of these cases being in men and 8.6 million in women [101]. According to WHO estimates, this number is expected to increase to over 14.5 million deaths from an estimated 24 million cancer cases by 2035 [102, 103]. That is nearly 1 in 6 of global deaths due to cancer, with approximately 70% of cancer deaths occurring in poor and less developed countries. For instance, one woman dies by cervical cancer every 8 min and one woman dies for every two women newly diagnosed with breast cancer in India [104]. As per the most recent globally estimated reports in 2018, nearly 400 types of cancers were recorded, with 28 types mostly seen as a problematic burden every day. In particular, lung (2.09 million), breast (2.09 M), colorectal (1.80 M), prostate (1.28 M), nonmelanoma skin (1.04 M) and stomach (1.03 M) cancers are the top 5 deadliest cancers in the world [105, 106]. Despite the majority of anticancer drugs currently available for the conventional chemotherapeutic treatments of human cancers being platinum based, there is still no standard amicable scientific solution to date because of the poor efficacy, non-selectivity and high toxicity of such drugs, which results in many inherent limitations, like neurotoxicity, nephrotoxicity, ototoxicity, tissue

toxicity, peripheral neuropathy, thrombocytopenia, neutropenia, nausea, emetogenesis and myelo suppression due to their interaction with DNA via covalent binding [107, 108]. Researchers are thus accelerating their efforts to invent novel synthetic roots to address the many challenges involved in the "war on cancer". In today's critical situation, there is an indispensable need to replace current drugs with appropriate alternatives to resolve the current limitations and to further the development and screening of potential anticancer agents with innovative strategies for the synthesis of less toxic alternatives, and to further identify potent and target specific drugs, which may preferably include non-covalent interactions [109].

4.4.1 Concept and principle of MTT assay:

This is a colorimetric assay that measures the reduction of yellow 3-(4,5-dimethythiazol- 2-yl)-2,5-diphenyl tetrazolium bromide (MTT) into an insoluble, coloured (dark purple) formazan product within the cell (*Fig. 4.18*). The cells are then solubilised with an organic solvent (e.g. DMSO) and the released, solubilised formazan reagent with an absorbance maximum near 570 nm is measured spectrophotometrically. Since reduction of MTT can only occur in metabolically active cells the level of activity is a measure of the viability of the cells. Viable cells with active metabolism convert MTT into formazan product but when cells die, they lose the ability to convert MTT into formazan, thus color formation serves as a useful and convenient marker of only the viable cells. The exact cellular mechanism of MTT reduction into formazan is not well understood. Speculation in the early literature involving specific mitochondrial enzymes has led to the assumption that MTT is measuring mitochondrial activity, the reduction being caused by mitochondrial succinate dehydrogenase, but most likely involves reaction with NADH or similar reducing molecules that transfer electrons to MTT [110-112].

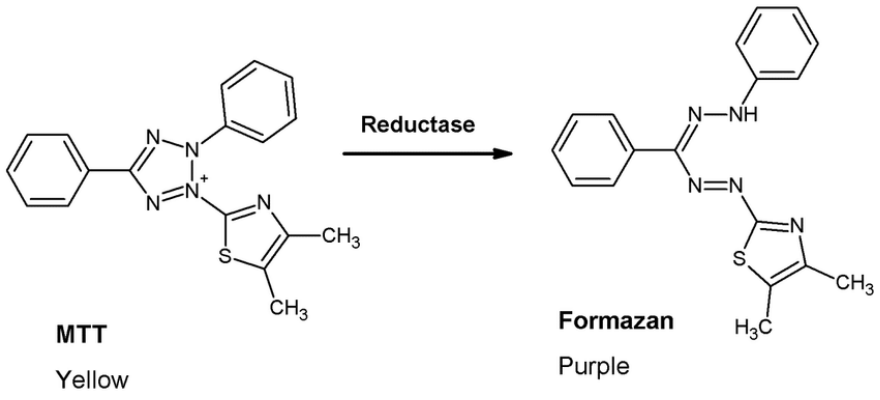

Fig. 4.19: *structure of MTT and colour formazan product*

4.4.2 Materials and instrumentation

The cell lines were cultured in Dulbecco's Modified Eagle Medium (DMEM), while Phosphate Buffer Saline (PBS) was used for washing purpose. The stock solutions of compounds (1 mg/ml) were prepared by first dissolving in minimum volume of DMSO (10µl) and then diluting the concentrated DMSO solution with DMEM media to 1 ml. Further dilutions from the stock solution were made using DMEM for subsequent dosing. The overall concentration of DMSO in the final sample was kept always lower than 1%. Both DMEM and PBS were purchased from Hi-Media. The MTT dye was purchased from SRL (Sisco research laboratory, Mumbai, India.). DMSO used to prepare stock solution as well as to dissolve formazan crystals was of analytical grade and purchased from Merck. 96-well culture plates were purchased from Tarson India Pvt. Ltd. The cell lines were procured from National Centre for Cell Science (NCCS), Pune, India. The spectrophotometric detection of culture plates was done by Biotek-ELX universal ELISA reader (Bio-Tek instruments, Inc., Winooski, VT). The data so obtained were converted into percentage viability and were analyzed and plotted with the help of the software Graphpad Prism 3 using one-way ANOVA as the statistical tool.

4.4.3 Experimental:

Cytotoxicity of the synthesised complexes was assessed by standard MTT colorimetric assay [113]. HeLa cells (5.0×10^3cells well^{-1}) were grown overnight in 96-well culture plates (Tarson India Pvt. Ltd.) at 37˚ C in a 5% CO_2 incubator. Binuclear complexes was added to the wells in the concentration range 0.5-150 mg/ml. Control wells containing only the culture medium without the compounds were prepared. The wells were incubated at 37˚ C in a 5% CO_2 incubator for 48 h and standard 3-(4,5-dimethylthiazole)-2,5-diphenyltetraazolium bromide (MTT) dye solution was then added to each well. After 4 h of incubation, the culture media was thrown away and the wells were washed with Phosphate Buffer Saline (Hi-Media, India Pvt. Ltd.) followed by addition of DMSO to dissolve the formazan crystals formed and further incubation for 30 min. The optical density of each well was measured spectrophotometrically at 563 nm using Biotek-ELX800MS universal ELISA reader (Bio-Tek instruments, Inc., Winooski, VT). The IC_{50} values were determined by plotting the percentage viability versus concentration on a logarithmic graph and reading off the concentration at which 50% of cells remained viable relative to the control. Each experiment was repeated at least three times to obtain mean values.

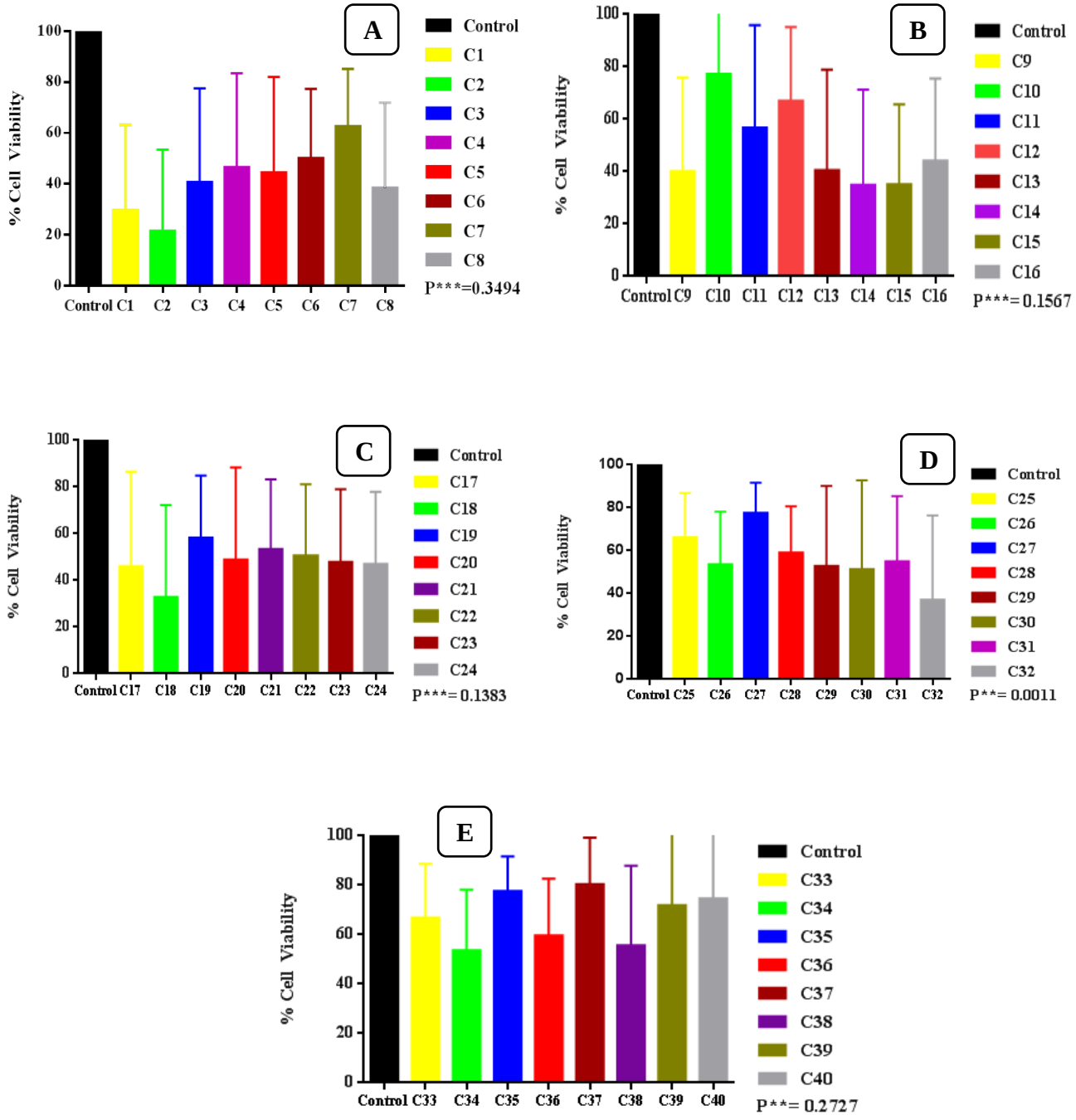

Fig. 4.20: *% Cell viability verses concentration plots of (A)* ***C1-8*** *(B)* ***C9-16*** *(C)* ***C17-24*** *(D)* ***C25-32*** *(E)* ***C33-40*** *on HeLa human cervical cancer cell line. Each point is the mean ± standard error obtained from three independent experiments*

4.4.4 Results and discussion:

In-vitro cytotoxicity tests of the binuclear ruthenium (II) arene complexes were performed on the human cervical cancer cell line (HeLa). The selection of this cell line was purely based on their higher occurrence in human population worldwide which is of prime concern. The cell viabilities (%) were obtained with continuous exposure of the cells to the said complexes for 48 h. The cytotoxicities of the complexes were found to be dose dependent, that is, the cell viability decreased with increasing concentrations (*Fig. 4.20*). The inhibitory concentration 50 (IC_{50}), is defined as the concentration required to reduce the size of the cell population by 50%. The IC_{50} values of the complexes have been tabulated in Table 4.11. It is observed that the complex **C18** with a ferrocenyl thiosemicarbazone ligand (IC_{50} = 4.2 ± 2.38 μM) is the most cytotoxic agent among all the various synthesized complexes. In general all the complexes in this series display low IC_{50} values and higher cytotoxicity. This may be attributed to the cumulative effect of the redox active ferrocenyl group and inhibition of ribonucletide reductase enzymes by the thiosemicarbazone moiety, both of which leads to their established cytotoxic activity against several cancer cell lines. The complexes of the diphenyl pyrazole amino acid conjugate series, **C9-C16** also exhibit low IC50 (μM) values in the order of **C14** (5.0 ± 3.7**)** < **C9** (9.1 ± 7.60) < **C13** (10.9 ± 1.48) < **C15** (12.4 ± 5.35) < **C17** (15.5 ± 8.11) < **C16** (15.7 ± 1.61) < **C10** (23.5 ± 8.27 < **C11** (32.6 ± 3.13) < **C12** (54.12 ± 3.70).

Several imidazole containing molecules have been reported to show cytotoxic activity against diverse cancer cell lines. The desirable electron-rich characteristics of the imidazole ring make possible its binding through diverse weak interactions with a variety of enzymes and receptors in biological systems. Imidazoles could interfere with DNA synthesis, and stop cell growth and division. So far, many imidazole derivatives as anticancer drugs such as dacarbazine (**1**), zoledronic acid (**2**), azathioprine (**3**), tipifarnib (**4**), and nilotinib (**5**) have been widely used in the clinic. They have been playing important roles in the treatment of various cancers [114]. Our studies revealed that the complexes with imidazole as bridging ligands display higher cytotoxity in general, towards the Hela cell lines compared to the complexes with 4, 4'azopyridine ligand.

Moreover, the complexes having greater cytotoxicity may probably be due to their higher solubility and disponibility in the culture medium [115]. There are reports in the literature on the cytotoxic effects of the complexes with longer incubation time periods (72 h) which may

result in the development of cellular resistance for that particular complex [116]. The data obtained for the complexes under study showed significant cytotoxicity with a short incubation period (48 h) which suggest that the complexes possess compelling activity against the tumor cell line. Although some of the synthesized binuclear ruthenium complexes are found to be less active compared to *cis* platin (IC_{50} ~ 18.8 μM) [117], they are much more active on cancer cells as compared to NAMI-A whose IC_{50} values have been found to be in the range of 608.5 μM for various cancer cell lines on treatment for 48 h [118] and those of RAPTA-C >1600 μM on treatment for 72 h [119]. The *in-vitro* anticancer activity of the compounds need not be consistent with their DNA/BSA-binding abilities. The different order of biomolecular binding affinity and the *in-vitro* anticancer activity means multiple targets and multiple mechanisms coexisted in the anticancer process of the compounds. DNA/serum albumin binding need not be the only target and mechanism for cytotoxicity. Moreover target mechanisms of the compounds may vary vividly whilst in a cellular environment [120].

Table 4.11 : IC_{50} values of complexes obtained from MTT assay on HeLa cell lines. Values have been expressed in **µM** concentrations. Reported values of cisplatin and known ruthenium complexes NAMI-A and RAPTA have been provided for reference.

Complexes code	***IC_{50} (µM)***	***Complexes code***	***IC_{50} (µM)***
C1	24.4 ± 2.96	**C25**	75.5 ± 5.77
C2	17.3 ± 1.82	**C26**	31.1± 6.17
C3	29.6 ± 5.14	**C27**	115.5±4.65
C4	31.7 ± 3.24	**C28**	32.3±8.51
C5	32.6 ± 2.04	**C29**	39.8 ±9.91
C6	35.9 ± 5.71	**C30**	43.4 ± 2.95
C7	41.3 ±11.44	**C31**	56.5 ± 5.12
C8	23.7 ± 8.90	**C32**	31.2 ± 2.56
C9	**9.1 ± 7.60**	**C33**	61.0 ± 2.98
C10	54.12 ± 3.70	**C34**	50.8 ± 6.70
C11	23.5 ± 8.27	**C35**	120.9 ± 4.65
C12	32.6 ± 3.13	**C36**	30.1 ± 8.51
C13	10.9 ± 1.48	**C37**	98.5 ± 6.29
C14	**5.0 ± 3.7**	**C38**	31.7 ± 3.51
C15	**6.4 ± 5.35**	**C39**	69.0 ± 2.98
C16	15.7 ± 1.61	**C40**	73.1 ± 6.70
C17	15.5 ± 8.11		
C18	**4.2 ± 2.38**	**Cisplatin**	18.8 ± 3.4
C19	21.6 ± 22.26	**NAMI-A**	608.5 ± 55.4
C20	17.8 ± 3.62	**RAPTA-C**	>1600
C21	30.2 ± 15.51		
C22	22.3 ± 2.07		
C23	14.5 ± 15.68		
C24	11.5 ± 5.40		

4.5 *Summary:*

All the binuclear Ru (II) complexes synthesized and presented in this thesis have been stepwise evaluated for their bioactivity. All the synthesised complexes were evaluated for DNA binding, protein binding and cytotoxicity studies. By using absorption and fluorescence spectral techniques, first the complexes have been checked for their interactions with DNA and BSA serum albumin which are the most commonly sought after biomolecular targets for anticancer activity. The results so obtained prompted to go for *in cellulo* studies. MTT assay gave an idea regarding the general cytotoxicity of the test complexes. The results of cytotoxicity study reveal a linear relationship between the concentration of the metal complexes and the percentage inhibition of HeLa cell growth without apparent damage to the cells in the absence of the complexes. Moreover, the cytotoxicity evaluation in vitro shows that complexes displayed better antitumor activity against the selected cell line, HeLa with a short incubation period.

4.6 *References:*

[1] Hurley, L. H. *Nat Rev Cancer*, **2002**, 2, 188.

[2] Paul, A.; Bhattacharya, S. *Current Sci.* **2012**, 102, 212.

[3] Cusumano, M.; Petro, M. L. D.; Giannetto, A.; Nicolo, F.; Rotondo, E. *Inorg. Chem.*, **1998**, 37, 563.

[4] Lerman, L. S. *J. Mol. Biol.* **1961**, 3, 18.

[5] Arena, G.; Scolaro, L. M.; Pasternack, R. F.; Romeo, R. *Inorg. Chem.*, **1995**, 34, 2994.

[6] Monaco, R. R. *J. Nucleic Acids*, **2010**, 702317.

[7] Pindur, U.; Haber, M.; Sattler, K. *J. Chem. Educ.*, **1993**, 70, 263.

[8] Werner, M. H.; Gronenborn, A. M.; Clore, G. M. *Science*, **1996**, 271, 778.

[9] Lincoln, P.; Nordén, B. *J. Phys. Chem. B*, **1998**, 102, 9583.

[10] Kostjukov, V. V.; Khomytova, N. M.; Hernandez Santiago, A. A.; Licona Ibarra, R.; Davies, D. B.; Evstigneev, M. P. *Int. J. Quantum Chem.*, **2011**, 111, 711.

[11] Mukherjee, A. *J. Phys. Chem. Lett.*, **2011**, 2, 3021.

[12] Zhang, S.; Ling, B.; Qu. F.; Sun, X. *Spectrochim. Acta, Part A*, **2012**, 97, 521.

[13] Pages, B.J.; Ang, D.L.; Wright, E.P.; Aldrich-Wright, J.R. *Dalton Trans*., **2015**, 44, 3505.

[14] Lowe, G.; Droz, A. S.; Vilaivan, T.; Weaver, G. W.; Park, J. J.; Pratt, J. M.; Tweedale, L.; Kelland, L. R. *J. Med. Chem.*, **1999**, 42, 3167.

[15] Farrell, N.; Qu. Y.; Hacker, M. P. *J. Med. Chem.*, **1990**, 33, 2179.

[16] Farrell, N. *Cancer Invest.*, **1993**, 11, 578.

[17] Mlcouskova, J.; Kasparkova, J.; Suchankova, T.; Komeda, S.; Brabec, V. *J. Inorg. Biochem.*, **2012**, 114, 15.

[18] Cepeda, V.; Fuertes, M. A.; Castilla, J.; Alonso, C.; Quevedo. C.; Perez, J. M. *Anti-Cancer Agents Med. Chem.*, **2007**, 7, 3.

[19] Muchova, T.; Quintal, S.; Farrell, N.; Brabec, V.; Kasparkova, J. *J. Biol. Inorg. Chem.*, **2012**, 17, 239.

[20] Cox, J. W.; Berners-Price, S. J.; Davies, M. S.; Qu, Y.; Farrell, N. *J. Am. Chem. Soc.*, **2001**, 123, 1316.

[21] Harris, A. L.; Yang, M.; Hegmans, A.; Povirk, L.; Ryan, J. J.; Kelland, L.; Farrell, N. *Inorg. Chem.*, **2005**, 44, 9598.

[22] Wang, K.; Gao, E. *Anti-Cancer Agents Med. Chem.*, **2014**, 14, 147.

[23] Pracharova, J.; Novakova, O.; Kasparkova, J.; Gibson, D.; Brabec, V. *Pure Appl. Chem.*, **2013**, 85, 343.

[24] Wheate, N. J.; Cullinane, C.; Webster, L. K.; Collins, J. G. *Anti-Cancer Drug Des.*, **2001**, 16, 91.

[25] Wheate, N. J.; Collins, J. G. *Anti-Cancer Agents Med. Chem.*, **2005**, 5, 267.

[26] Ongoma, P. O.; Jaganyi, D. *Int. J. Chem. Kinet.*, **2013**, 45, 676.

[27] Reedijk, J. *Platinum Met. Rev.*, **2008**, 52, 2.

[28] Lowe, G.; Droz, A. S.; Vilaivan, T.; Weaver, G. W.; Park, J. J.; Pratt, J. M.; Tweedale, L.; Kelland, L. R. *J. Med. Chem.*, **1999**, 42, 3167.

[29] Chan, H. -L.; Ma, D. -L.; Yang, M.; Che, C. M. *Chem Bio. Chem*., **2003**, 4, 62.
[30] Piccart, M. J.; Lamb, H.; Vermorken, J. B. *Ann. Oncol.*, **2001**, 12, 1195.

[31] Arnott, S. *Nature*, **1986**, 320, 313.

[32] Oguey, C.; Foloppe, N.; Hartmann, B. *PLoS One*, **2010**, 5, 15931.

[33] Sinden, R. R. DNA Structure and Function, Academic Press, Sydney, 1994.

[34] Privalov, P. L.; Dragan, A. I.; Crane-Robinson, C.; Breslauer, K. J.; Remeta, D. P.; Minetti, C. A. S. A. *J. Mol. Biol.*, **2007**, 365, 1.

[35] Komeda, S.; Moulaei, T.; Woods, K. K.; Chikuma, M.; Farrell, N. P.; Williams, L. D. *J. Am. Chem. Soc.*, **2006**, 128, 16092.

[36] Hayward, R. L.; Schornagel, Q. C.; Tente, R.; Macpherson, J. S.; Aird, R. E.; Guichard, S.; Habtemariam, A.; Sadler, P.; Jodrell, D. I. *Cancer Chemother. Pharmacol.*, **2005**, 55, 577.

[37] Trudu, F.; Amato, F.; Vaňhara, P.; Pivetta, T.; Peña-Méndez, E. M.; Havel, J. *J. Appl. Biomed.*, **2015**, 13, 79.

[38] Ang, W. H.; Dyson, P. J. *Eur. J. Inorg. Chem.*, **2006**, 2006, 4003.

[39] Liu, H.K.; Berners-Price, S.J.; Wang, F.; Parkinson, J.A.; Xu, J.; Bella, J.; Sadler, P. J. *Angew. Chem. Int. Ed.*, **2006**, 45, 8153.

[40] Habtemariam, A.; Melchart, M.; Fernández, R.; Parsons, S.; Oswald, I. D. H.; Parkin, A.; Fabbiani, F. P. A.; Davidson, J. E.; Dawson, A.; Aird, R. E.; Jodrell, D. I.; Sadler, P. J. *J. Med. Chem.*, **2006**, 49, 6858.

[41] Yan, Y. K.; Melchart, M.; Habtemariam, A.; Sadler, P. J. *Chem Commun.*, **2005**, 4764.

[42] Peacock, A. F. A.; Parsons, S.; Sadler, P. J. *J. Am. Chem. Soc.*, **2007**, 129, 3348.

[43] Dyson, P. J.; Sava, G. *Dalton Trans.*, **2006**, 1929.

[44] Timerbaev, A. R.; Hartinger, C. G.; Aleksenko, S. S.; Keppler, B. K. *Chem Rev.*, **2006**, 106, 2224.

[45] Huang, Y. C.; Haribabu, J.; Chien, C. M.; Sabapathi, G.; Hsu, S. C. N. *J. Inorg. Bioch.*, **2019**, 194, 74.

[46] Paira, P.; Anuja, P. K. *J. Inorg. Bioch.*, **2020**, 208, 111099.

[47] Wu, Q.; Liu, L.Y.; Li, S.; Wang, F.X.; Li, J.; Qian, Y.; Su, Z.; Mao, Z. W.; Sadler, P. J.; Liu, H. K. *J. Inorg. Bioch.*, **2018**, 189, 30.

[48] Colina-Vegas, L.; Luna-Dulcey, L.; Plutín, A. M.; Castellano, E. E.; Cominetti, M. R.; Batista, A. A. *Dalton transaction*, **2017**, 46, 12865.

[49] Jeyalakshmi, K.; Haribabu, J.; Balachandran, C.; Swaminathan, S.; Bhuvanesh, N. S. P.; Karvembu, R. *Organometallics*, **2019**, 38, 753.

[50] Kesicki, E. A.; DeRcwch, M. A.; Freeman, L. H.; Walton, C. L.; Harvey, D. F.; Trogler, W. C. *Inorg. Chem.*, **1993**, 32, 5851.

[51] Marmur, J. *J. Mol. Biol*., **1961**, *3*, 208.

[52] Reichmann, M.F.; Rice, S.A.; Thomas, C.A.; Doty, P. *J. Am. Chem. Soc*., **1954**, 76, 3047.

[53] Son, G.; Yeo, J.; Kim, M.; Kim, S.; Holmen, A.; Akerman, B.; Norden, B. *J. Amer. Chem. Soc.*, **1998**, 120, 6451.

[54] Xiao, Y.N.; Zhan, C.X. *J. Appl. Polym. Sci*., **2002**, 84, 887.

[55] Sohrabi, N. *J. Pharm. Sci. & Res.*, **2015**, 7, 533.

[56] Tabassum, S.; Asbahy, W. M.; Afzal, M.; Arjmand, F. *J. of Luminescence*, **2012**, 132, 3058.

[57] Pyle, A. M.; Rehmann, J. P.; Meshoyrer, R.; Kumar, C. V.; Turro, N. J.; Barton, J. K. *J. Am. Chem. Soc.*, **1989**, 111, 3051.

[58] Laila, H.; Rahman, A.; Rafat, M.; Khatib, E. I.; Nassr, L. A. B.; Abu-Dief, A. M.; Ismael, M.; Seleem, A. A. *Spectrochimica Acta Part A: Molecular and Biomolecular Spectroscopy*, **2014**, 117**,** 366.

[59] Dimitrakopoulou, A.; Dendrinou-Samara, C.; Pantazaki, A. A.; Alexiou, M.; Nordlander, E.; Kessissoglou, D. P. *J. Inorg. Biochem*., **2008**, 102, 618.

[60] Zhao, G.; Lin, H.; Zhu, S.; Sun, H.; Chen, Y. *J. Inorg. Biochem.*, **1998**, 70, 219.

[61] Dhar, S.; Nethaji, M.; Chakravarty, A. R. *J. Inorg. Biochem*., **2005**, 99, 805.

[62] Baguley, B. C.; Falkenhaug, E. M. *Nucleic Acids Res.*, **1978**, 5, 161.

[63] Boger, D.L.; Fink, B. E.; Brunette, S. R.; Tse, W. C.; Hedrick, M. P. *J. Am. Chem. Soc.*, **2001**, 123, 5878.

[64] Pasternack, R. F.; Cacca, M.; Keogh, B.; Stephenson, T. A.; Williams, A. P.; Gibbs, F. J. *J. Am. Chem. Soc.*, **1991**, 113, 6835.

[65] Lakowicz, J. R.; Weber, G. *Biochemistry*, **1973**, 12, 4161.

[66] Satyanarayana, S.; Dabrowiak, J. C.; Chaires, J. B. *Biochemistry*, **1993**, 32, 2573.

[67] Suh, D.; Chaires, J. B. *Bioorg. Med. Chem.*, **1995**, 3, 723.

[68] Kelly, J. M.; Tossi, A. B.; McConnell, D. J. *Nucleic Acids Res.*, **1985**, 13, 6017.

[69] Patel, M. N.; Patel, C. R.; Joshi, H. N.; Thakor, K. P. *Spectrochim. Acta Part A*, **2014**, 127, 261.

[70] Lee, S. K.; Nam, K. A.; Hoe, Y. H.; Min, H. -Y.; Kim, E. -Y.; Ko, H.; Song, S.; Lee, T.; Kim, S. *Arch. Pharm Res.*, **2003**, 26, 253.

[71] Moradi, Z.; Khorasani-Motlagh, M.; Rezvani, A. R.; Noroozifar, M. *J. Biomol. Structure and Dynamics*, **2017**, 36, 779.

[72] Peterson, L. R. *Clinical Infectious Diseases*, **2001**, 33, S180.

[73] Topală, T.; Bodoki, A.; Oprean, L.; Oprean, R. *Clujul Medical*, **2014**, 87, 215.

[74] Liu, H.; Shi, X.; Xu, M.; Li, Z.; Huang, J.; Bai, D.; *Eur J Med Chem.*, **2011**, 46, 1638.

[75] Sathyadevi, P.; Krishnamoorthy, P.; Jayanthi, E.; Butorac, R. R.; Cowley, A. H.; Dharmaraj, N. *Inorganica Chimica Acta.*, **2012**, 384, 83.

[76] Urquiza, N. M.; Naso, L. G.; Manca, S. G.; Lezama, L.; Rojo, T.; Williams, P. A. M.; Ferrer, E. G. *Polyhedron.*, **2012**, 31, 530.

[77] Xiang, Y.; Wu, F. *Spectrochim Acta A Mol Biomol Spectrosc.*, **2010**, 77, 430.

[78] Peters T. J. *Biochemistry, Genetics, and Medical Applications*, **1995**, 9.

[79] Majorek, K. A.; Porebski, P. J.; Dayal, A.; Zimmerman, M. D.; Jablonska, K.; Stewart, A. J.; Chruszcz, M.; Minor, W. *Mol. Immunol.*, **2012**, 52, 174.

[80] Jalali, F.; Dorraji, P. S.; Mahdiuni, H. *Journal of Luminescence.*, **2014**, 148, 347.

[81] Bal, W.; Christodoulou, J.; Sadler, P.J.; Tucker, A. *J Inorg Biochem.*, **1998**, 70, 33.

[82] Gharagozlou, M.; Boghaei, D. M. *Spectrochim Acta A Mol Biomol Spectrosc.*, **2008**, 71, 1617.

[83] Krishnamoorthy, P.; Sathyadevi, P.; Cowley, A. H.; Butorac, R. R.; Dharmaraj, N. *Eur J Med Chem.*, **2011**, 46, 3376.

[84] Ehteshami, M.; Rasoulzadeh, F.; Mahboob, S.; Rashidi, M. R. *Journal of Luminescence.*, **2013**, 135, 164.

[85] Vignesh, G.; Arunachalam, S.; Vignesh, S.; James, R. A. *Spectrochim Acta A Mol Biomol Spectrosc.*, **2012**, 96, 108.

[86] Ray, A.; Koley Seth, B.; Pal, U.; Basu, S. *Spectrochim Acta A Mol Biomol Spectrosc.*, **2012**, 92, 164.

[87] Eftink, M. R.; Ghiron, C. A. *Anal Biochem.*, **1981**, 114, 199.

[88] Samari, F.; Hemmateenejad, B.; Shamsipur, M.; Rashidi, M.; Samouei, H. *Inorg Chem.*, **2012**, 51, 3454.

[89] Sathyadevi, P.; Krishnamoorthy, P.; Butorac, R. R.; Cowley, A. H.; Bhuvanesh, N. S. P.; Dharmaraj, N. *Dalton Trans.*, **2011**, 40, 9690.

[90] Xue, F.; Xie, C. Z.; Zhang, Y. W.; Qiao, Z.; Qiao, X.; Xu, J. Y.; Yan, S. P. *J Inorg Biochem.*, **2012**, 115, 78.

[91] Asadi, M.; Asadi, Z.; Zarei, L.; Sadi, S. B.; Amirghofran, Z. *Spectrochim Acta A Mol Biomol Spectrosc.*, **2014**, 133, 697.

[92] Ni, Y.; Su, S.; Kokot, S. *Anal Chim Acta.*, **2006**, 580, 206.

[93] Zahirović, A.; Žilić, D.; Pavelić, S. K.; Hukić, M.; Muratović, S.; Harej, A.; Kahrović, E. *New J. Chem.*, **2019**, **43**, 5791.

[94] Lakowicz, J. R. *Principles of Fluorescence Spectroscopy*, 2nd Ed., Plenum Press, New York, **1999**.

[95] Goswami, T. K.; Chakravarthi, B. V. S. K.; Roy, M.; Karande, A. A.; Chakravarty, A. R. *Inorg. Chem.*, **2011**, 50, 8452.

[96] Anjomshoa, M.; Fatemi, S. J.; Torkzadeh-Mahani, M.; Hadadzadeh, H. *Spectrochimica Acta Part A: Molecular and Biomolecular Spectroscopy*, **2014**, 127, 511.

[97] Rajendiran, V.; Karthik, R.; Palaniandavar, M.; Periasamy, V. S.; Akbarsha, M. A.; Srinag, B. S. *Inorg Chem.*, **2007**, 46, 8208

.

[98] Tarushi, A.; Totta, X.; Papadopoulos, A.; Kljun, J.; Turel, I.; Kessissoglou, D. P. *Eur J Med Chem.*, **2014**, 74, 187.

[99] Li, Y.; Li, Y.; Wang, N.; Lin, D.; Liu, X.; Yang, Y.; Gao, Q. *J. Biomol. Struct. Dyn.*, **2019**. 1.

[100] Mishra, B.; Barik, A.; Priyadarsini, K. I.; Mohan, H. *J. Chem. Sci.*, **2005**, 117, 641.

[101] Siegel, R.L.; Miller, K.D.; Jemal, A. *Ca-Cancer J. Clin*., **2018,** 68, 7.

[102] Reddy, K.S.; *Lancet*, **2016**, 388, 1448.

[103] Liu, H.W.; Chen, L.; Xu, C.; Li, Z.; Zhang, H.; Zhang, X.B.; Tan, W. *Chem. Soc. Rev*., **2018**, 47, 7140.

[104] Bray, F.; Ren, J.S.; Masuyer, E.; Ferlay, J. *Int. J. Cancer*, **2012**, 132, 1133.

[105] GBD 2015 Maternal Mortality Collaborators, *Obstet. Gynecol. Surv*., **2017**, 72, 11.

[106] Subarkhan, M. K. M.; Ramesh, R. *Inorg. Chem. Front*., **2016**, 3, 1245.

[107] Kasim, M. S. M.; Sundar, S.; Rengan, R. *Inorg. Chem. Front*., **2018**, 5, 585.

[108] Ma, W.; Tian, Z.; Zhang, S.; He, X.; Li, J.; Xia, X.; Chen, X.; Liu, Z. *Inorg. Chem. Front.*, **2018**, 5, 2587.

[109] Zhang, Y.; Luo, Q.; Zheng, W.; Wang, Z.; Lin, Y.; Zhang, E.; Lu, S.; Xiang, J.; Zhao, Y.; Wang, F. *Inorg. Chem. Front*., **2018**, 5, 413.

[110] Berridge, M. V.; Tan, A. S. *Arch. Biochem. Biophys.*, **1993**, 303, 474.

[111] Berridge, M.; Tan, A.; McCoy, K.; Wang, R. *Biochemica*, **1996**, 4, 14.

[112] Marshall, N. J.; Goodwin, C. J.; Holt, S. *J. Growth Regul.*, **1995**, 5, 69.

[113] Mosmann, T. *J. Immunol. Methods*, 1983, 65, 55.

[114] Sharma, G. V.M.; Ramesh, A.; Singh, A.; Srikanth, G.; Jayaram', V.; Duscharla, D.; Jun, J.H.; Ummanni, R.; Malhotra, S.V. *Med. Chem. Commun*., **2014**, 5, 1751.

[115] Silva, E.N.D.; Silva, P.A.B.D.; Graminha, A. E.; Oliveira, P.F.D.; Damasceno, J. L.; Tavares, D. C.; Batista, A.A.; Poelhsitz, G.V. *Bioinorg. Chem. App*. **2017**, 2017, 1, Article ID 2562780.

[116] Ramachandran, E.; Thomas, S.P.; Poornima, P.; Kalaivani, P.; Prabhakaran, R.; Padma, V.V.; Natarajan, K. *Eur. J. Med. Chem*., **2012**, 50, 405.

[117] Tan, C.; Hu, S.; Liu, J.; Liangnian, J. *Eur. J. Med. Chem*., **2011**, 46, 1555.

[118] Petra, H.; Bock, K.; Atil, B.; Hoda, M.A.; Korner, W.; Bartel, C.; Jungwirth, U.; Keppler, B.K.; Michael, M.; Berger, W.; Gunda, K. *J. Biol. Inorg. Chem*., 2010, 15, 737.

[119] Wee, H.A.; Elisa, D.; Claudine, S.; Rosario, S.; Lucienne, J.; Dyson, P. *J. Inorg. Chem*., 2006, 45, 9006.

[120] Ramadevi, P.; Singh, R.; Jana, S.S.; Devkar, R.; Chakraborty, D. *J. Photochem. Photobiol. A: Chem.*, **2015**, 305, 1.